



## **JGR** Oceans

#### RESEARCH ARTICLE

10.1029/2022JC018462

#### **Key Points:**

- Wind opposing the direction of Kelvin wave propagation can enhance near- and midfield mixing in small- to midsized tidal plumes
- Advection of plume and ambient stratification offshore and enhanced wind straining contribute to larger mixing rates
- The largest mixing events are linked to shelf stratification, while straining and advection are linked to instantaneous wind direction

#### Correspondence to:

P. Spicer, preston.spicer@maine.edu

#### Citation:

Spicer, P., Cole, K. L., Huguenard, K., MacDonald, D. G., & Whitney, M. M. (2022). Wind effects on near-and midfield mixing in tidally pulsed river plumes. *Journal of Geophysical Research: Oceans*, 127, e2022JC018462. https://doi.org/10.1029/2022JC018462

Received 20 JAN 2022 Accepted 9 MAY 2022

# © 2022. The Authors. This is an open access article under the terms of the Creative Commons Attribution License, which permits use, distribution and reproduction in any medium, provided the original work is properly cited.

# Wind Effects on Near- and Midfield Mixing in Tidally Pulsed River Plumes

Preston Spicer<sup>1</sup>, Kelly L. Cole<sup>1</sup>, Kimberly Huguenard<sup>1</sup>, Daniel G. MacDonald<sup>2,3</sup>, and Michael M. Whitney<sup>4</sup>

<sup>1</sup>Department of Civil and Environmental Engineering, University of Maine, Orono, ME, USA, <sup>2</sup>Department of Estuarine and Ocean Science, School for Marine Science and Technology, University of Massachusetts Dartmouth, Dartmouth, MA, USA, <sup>3</sup>Department of Civil and Environmental Engineering, University of Massachusetts Dartmouth, Dartmouth, MA, USA, <sup>4</sup>Department of Marine Sciences, University of Connecticut, Groton, CT, USA

**Abstract** River plumes transport and mix land-based tracers into the ocean. In tidally pulsed river plumes, wind effects have long been considered negligible in modulating interfacial mixing in the energetic nearfield region. This research tests the influence of variable, realistic winds on mixing in the interior plume. A numerical model of the Merrimack River plume-shelf system is utilized, with an application of the salinity variance approach employed to identify spatial and temporal variation in advection, straining, and dissipation (mixing) of vertical salinity variance (stratification). Results indicate that moderate wind stresses (~0.5 Pa) with a northward component countering the downcoast rotation of the plume are most effective at decreasing stratification in the domain relative to other wind conditions. Northward winds advect plume and ambient shelf stratification offshore, allowing shelf water salinity to increase in the nearshore, which strengthens the density gradient at the plume base. Straining in the plume increases with winds enhancing offshore-directed surface velocities, leading to increased shear at the plume base. Increased straining and larger density gradients at the plume base enhance variance dissipation in the near- and midfield plume, and dissipation remains enhanced if the shelf is clear of residual stratification. The smaller spatial and temporal scales of the Merrimack plume allow the mechanisms to occur at tidal time scales in direct response to instantaneous winds. This is the first study to show tidal time scale wind-induced straining and advection as controlling factors on near- and midfield mixing rates in river plumes under realistic winds.

Plain Language Summary Rivers transport pollutants, nutrients, and sediments into the ocean. Often, fresh water from rivers spread out over the denser, salty ocean water, creating a river plume. How these plumes mix and move under different environmental conditions is important to understand for accurate tracing of river-borne materials into the ocean. In river plumes which form anew on each ebbing, seaward-directed tide (called tidally pulsed), winds have often been considered unimportant to mixing relative to tidal mixing. In this work, a numerical model of the tidally pulsed Merrimack River plume is used to test that assumption. Mixing in the energetic plume interior can, in fact, be enhanced during specific wind conditions, when the plume and coastal ocean surface waters are pushed offshore, the plume moves faster than normal, and the salinity difference from surface to bottom increases. Essentially, wind can control differences in density under the plume and how quickly the plume moves, both of which influence vertical mixing. The results presented are particularly applicable for smaller plumes over shallower water which are not influenced by larger scale ocean dynamics.

#### 1. Introduction

The discharge of river-borne water into the coastal ocean is subject to a variety of physical processes which mix fresh and salty water. Mixing dictates pollutant, nutrient, and sediment fate and so can influence coastal ecological health. In general, plumes mix into the coastal ocean by wind, waves, tidal processes, and frontal shear and convergence at plume interfaces (Horner-Devine et al., 2015). Although great advances have been made in recent years observing and modeling plumes, there is still significant uncertainty regarding the importance of mixing mechanisms spatially and temporally in plumes exposed to different environmental conditions.

Coastal winds are a notable environmental condition controlling plume dynamics. Winds can modify circulation patterns over the shelf, which in turn modulate river plume dynamics outside the estuary. Extensive numerical and

SPICER ET AL. 1 of 21

analytical work have determined upwelling and downwelling favorable wind events, created via along-shelf wind stresses, are important to the vertical and horizontal extent of plume structure and mixing. Upwelling winds often thin plumes and advect them offshore via Ekman transport, leading to significant mixing because of increased vertical shear in horizontal currents (Fong & Geyer, 2001; Lentz, 2004; Whitney & Garvine, 2005). Downwelling winds can augment down-shelf currents, attach plumes to the shore, and subsequently mix the water column by entraining ambient waters into the plume (Moffat & Lentz, 2012; Whitney & Garvine, 2005) or by inducing cross-shore upwelling circulation within the coastal-trapped current (S. Y. Chen & Chen, 2017). Recently, modeling work has expanded to test the impact of cross-shelf winds (Jurisa & Chant, 2013; Tilburg, 2003; Zhang et al., 2014) to plume mixing, finding mixing to be typically determined by the cross-shore advection of salt and the downstream transport of freshwater. However, the research related to along- and cross-shelf winds generally focus on large time scale (multiple days) Ekman responses or idealized wind forcing. Realistic winds are often short in duration and variable and can create plume responses which differ from large-scale Ekman theory (Hunter et al., 2010). It is yet to be determined how important to mixing and stratification realistic, shorter time scale wind forcing can be in smaller, tidal time scale plumes, particularly in their often energetic near- and midfield regions.

Tidally pulsed plumes occur in regions with significant tidal energy, creating an estuary discharge dominated by tides and discharge momentum flux (e.g., the Connecticut River and River Teign plumes). Generally, this manifests as a "new" surface-advected plume every ebb tide which spreads over denser shelf waters. Unlike larger, nontidal plumes (e.g., the Mississippi River and Amazon River plumes), the dynamic near- and midfield regions of tidally pulsed systems often form and evolve on a tidal time scale which creates intratidal variability in dynamics (Horner-Devine et al., 2015). The nearfield is defined as the region near the river mouth where estuary discharge momentum dominates dynamics and generally features the most intense mixing at the very sheared and stratified plume base (Hetland, 2010; Hetland & MacDonald, 2008; MacDonald et al., 2007). The midfield marks the region when Earth's rotation becomes influential and starts turning the plume downcoast of the river mouth (Garvine, 1987; Horner-Devine et al., 2015). Preliminary mixing budgets in tidally pulsed plumes have estimated nearly 50% of mixing during a tidal pulse occurs within the near- and midfield plume (Spicer et al., 2021), outlining the importance of these energetic regions to net plume mixing. The nearfield is considered particularly sensitive to tides (Nash et al., 2009; Spahn et al., 2009) and so wind effects there are often considered negligible in tidal plumes (Horner-Devine et al., 2009). It is in the midfield that wind effects are generally thought to become important in response to longer time scale Ekman dynamics. Recent observations in the tidal Merrimack River plume indicate that tidal time scale nearfield transport is more sensitive to local winds than previously assumed and it is hypothesized that mixing is sensitive to wind as well (Kakoulaki et al., 2014).

At present, a handful of observational studies have investigated plume dynamics in the near- and midfield of tidally pulsed plumes under realistic wind forcing (Flores et al., 2017; Kastner et al., 2018; Rijnsburger et al., 2018). Notably, a drifter observational program performed by Kastner et al. (2018) was the first to estimate mixing along streamlines in the near- and midfield Fraser River plume under realistic winds. Markedly different mixing regimes were determined based on wind direction which the authors attribute to modifications in plume geometry. Although novel, the former work is restricted in spatial and temporal resolution which limits the diagnosis of mixing mechanisms. Further, wind effects on one particular tidal plume have not been connected to the dynamics of succeeding plumes. As of yet, a direct evaluation of plume mixing mechanisms on a tidal time scale under varying, realistic winds has yet to be achieved, particularly for successive tidal pulses.

Quantifying direct relationships between the formation and fate (transport and/or mixing) of stratification generally provides a more complete evaluation of mixing in coastal systems. Multiple techniques have been utilized in recent years to better quantify the evolution of stratification. Budgets based on the buoyancy flux and potential energy anomaly (PEA) equation (Burchard & Hofmeister, 2008; Simpson et al., 1990) have been popularly used. Although useful, the PEA methods applied to river plumes are often complicated to formulate (de Boer et al., 2008) or indirectly relate the formation of stratification to mixing (Pritchard & Huntley, 2006; Spicer et al., 2021). The salinity variance equation has recently become a more widely accepted and refined method to evaluate stratification and mixing (Burchard & Rennau, 2008; Li et al., 2018; MacCready et al., 2018; Warner et al., 2020) but has mainly been applied to estuaries. The salinity variance approach is simple in formulation and allows for direct comparisons between net changes in stratification to transport (advection) and destruction (dissipation/mixing) of stratification. Further, the transformation of salinity variance model (Li et al., 2018) adds an additional term which quantifies the creation of stratification through straining of horizontal density gradients.

SPICER ET AL. 2 of 21

21699291, 2022, 5, Downloaded from https://agupubs.onlinelibrary.wiley.com/doi/10.1029/2022IC018462, Wiley Online Library on [09/05/2023]. See the Terms and Conditions (https://onlinelibrary.wiley.com/doi/10.1029/2022IC018462, Wiley Online Library on [09/05/2023]. See the Terms and Conditions (https://onlinelibrary.wiley.com/doi/10.1029/2022IC018462, Wiley.com/doi/10.1029/2022IC018462, Wiley.com/doi/10.1029/20218462, Wiley.com/doi/10.1029/20218462, Wiley.com

and-conditions) on Wiley Online Library for rules of use; OA articles are governed by the applicable Creative Commons License

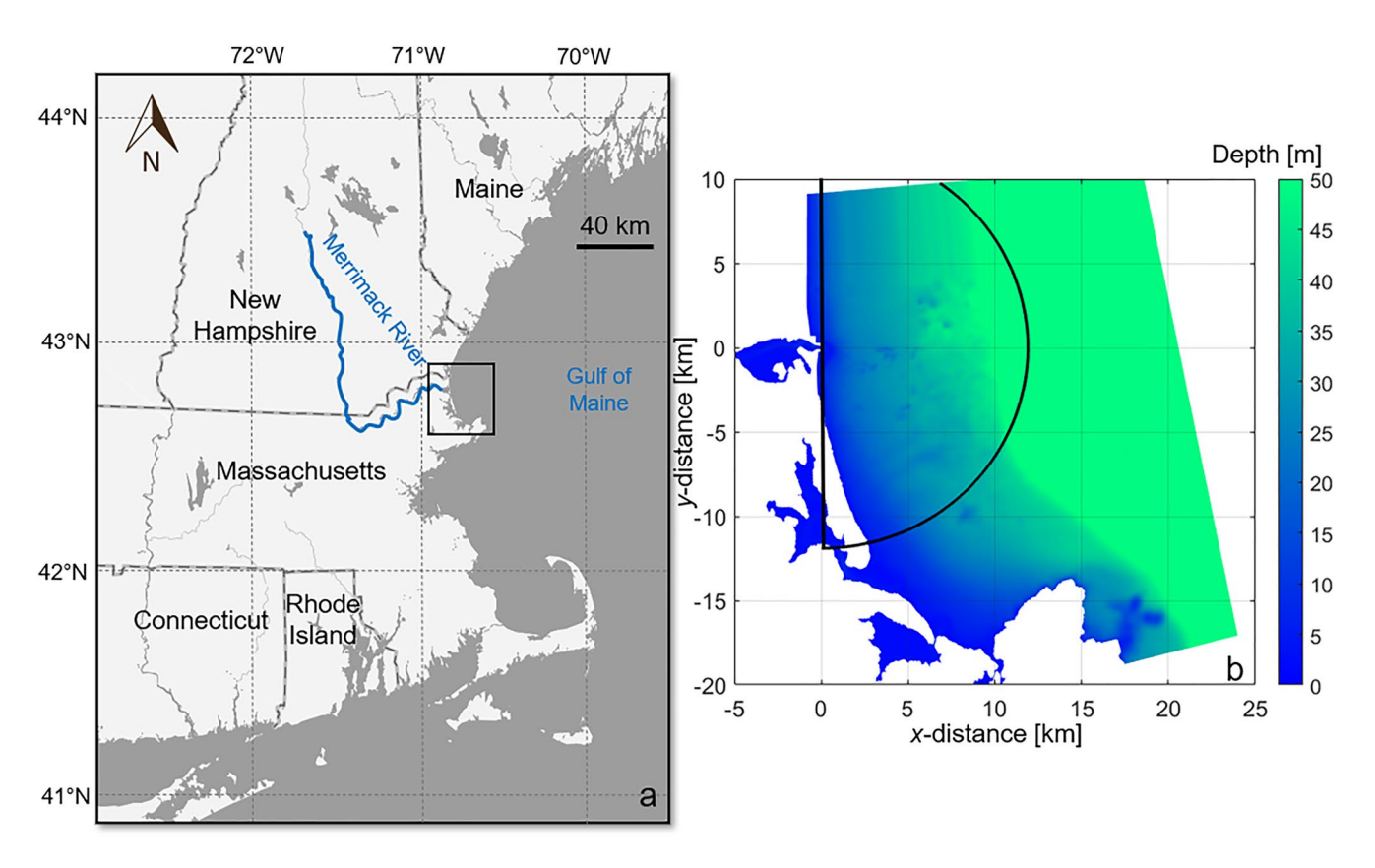


**Figure 1.** (a) The Merrimack River (blue) shown relative to the Gulf of Maine and surrounding states. (b) Zoom in (black box in panel a) at the mouth of the Merrimack River. Model bathymetry is shown as filled colored contours and the control volume region used in formulating salinity variance terms is outlined in black. The horizontal axis in panel (b) is the *x*-distance from the river mouth and the vertical is the *y*-distance.

This technique allows for robust spatial and temporal variability in advection, mixing, and straining to be determined and has yet to be applied in analyzing a tidally pulsed river plume.

In this paper, we study the Merrimack River plume, a surface-advected tidal plume which spreads and mixes into the Gulf of Maine. The gently sloping, uncomplicated, and shallow shelf bathymetry has made the Merrimack a popular natural laboratory for the study of tidally pulsed plumes over recent years (e.g., Cole et al., 2020; Hetland & MacDonald, 2008; MacDonald et al., 2007). The aim of this work is to evaluate stratifying and destratifying processes in the near- and midfield of a tidally pulsed river plume exposed to realistic wind forcing. The objectives of this study are to (a) quantify the net influence of straining, advection, and mixing on tidal plume stratification under realistic winds and (b) evaluate the mechanisms responsible for variability in mixing within the near- and midfield plume regions over multiple tidal pulses under differing winds. The Merrimack River plume model is described in detail in Section 2.1, an overview of the transformation of salinity variance equation used to evaluate stratification and mixing is given in Section 2.2, and results outlining significant decreases in stratification over the domain following wind events with a northerly component are presented in Sections 3.1–3.3. In Section 3.4, we diagnose the mechanisms which contribute to increased mixing during those wind events, then expand, and verify those mechanisms using the entire analysis period in Section 3.5. A discussion relating this work to others is given in Section 4, and conclusions are presented last in Section 5.

#### 2. Methods

#### 2.1. Model

Realistic simulations of the Merrimack River estuary–shelf system (Figure 1) are used in this study. During periods of moderate to high discharge (300–700 m³/s), the Merrimack River outflow produces a classic, radially

SPICER ET AL. 3 of 21

expanding, tidally pulsed river plume. The Merrimack River plume model used in this work has been applied and validated in other works studying tidal plume hydrodynamics and mixing (F. Chen et al., 2009; Hetland & MacDonald, 2008).

Simulations are created using the Regional Ocean Modeling System (ROMS; Haidvogel et al., 2008; Shchepetkin & McWilliams, 2005), which is a free-surface, hydrostatic, primitive equation ocean model using terrain-following sigma coordinates. A curvilinear grid of the north coast of Massachusetts and New Hampshire (Figure 1b) is utilized which applies realistic bathymetry and coastal morphology to represent the Merrimack River outflow region. The grid encompasses a region 10 km upstream in the estuary to 20 km offshore with similar 10 and 20 km (from the river mouth) upcoast and downcoast limits, respectively. Grid resolution is 40 m at the mouth and expands to 100 m at the offshore boundaries. Thirty vertical sigma layers define depth coordinates everywhere in the domain and are controlled by stretching parameters,  $\theta$ , of 1 and 0.5 for the surface and bottom, respectively, with a critical depth of 3 m, thereby focusing resolution in the top 3 m of the water column. The estuary depth is 6 m at the mouth and 300 m wide. Roughly 500 m seaward from the mouth is a slightly shallower sill where freshwater detaches from the bottom and the surface-advected river plume forms during sufficient flows.

The MPDATA scheme is used to describe horizontal and vertical tracer advection in each simulation and is considered a nonoscillatory Lax–Wendroff scheme which focuses on sign preserving multidimensional advection as opposed to monotone solutions in one dimension (Smolarkiewicz & Grabowski, 1990). MPDATA can produce modest numerical mixing relative to other advection schemes (i.e., U3H), but more accurately preserves tracer quantities and is considered suitable for estuary and river plume applications (Kalra et al., 2019). A Flather condition is used at each oceanic boundary for 2-D velocities and the free surface (Flather, 1975), while an Orlanski condition is used for 3-D velocities and salt/temperature tracers (Orlanski, 1976). Vertical mixing is determined using the k–ε turbulence closure scheme (Umlauf & Burchard, 2003) with Canuto-A stability functions (Canuto et al., 2001). Former work has shown the model to be relatively insensitive to choice of turbulence closure (MacDonald et al., 2007). The momentum equation uses quadratic bottom friction with conservative, parabolic spline reconstruction applied to vertical derivatives in the model.

These ROMS simulations use the hydrostatic assumption, thereby neglecting convective instabilities. It is likely that mixing in the plume front could include significant convective instabilities, and so some error could exist in dissipation of variance or straining estimates there. The front is spatially small relative to the near- and midfield plume, though (estimates range from 10 to 260 m wide in other tidal plumes, but likely vary significantly between systems [Horner-Devine et al., 2015; Huguenard et al., 2016]), and has been hypothesized to be unimportant in dictating net plume dynamics (such as mixing) in former work (Cole et al., 2020; Spicer et al., 2021). For these reasons, the results of this paper would likely be unaffected by a front modeled using a nonhydrostatic formulation.

River discharge is determined from a USGS gage in Lowell, MA (station #01100000) and is prescribed to the western boundary of the domain as a 0 psu, 10°C inflow. The initial shelf condition is set to 32 psu salinity with a temperature of 7°C, typical of early spring, and is not vertically stratified. Temperature-driven variation to stratification and mixing is considered negligible relative to salinity-driven variation for the given ranges. Throughout the model simulation, the 0 psu river discharge is consistently input to the system according to the discharge rates described below. At the oceanic boundaries, no vertical gradients in salinity or temperature are applied or input to the system. No air-sea exchange occurs which could create freshwater or heat fluxes at the surface. All freshwater fluxes (and negligible heat fluxes) are therefore driven by river input, making simulations slightly idealized, as other freshwater and heat fluxes could be introduced at the ocean boundaries in nature. Wind stresses are applied to the entire domain and are from a NOAA meteorological station on the Isle of Shoals (sampled hourly, station IOSN3) in New Hampshire, approximately 25 km northeast of the estuary. Tides are predicted by Xtide, a harmonic tide clock and time predictor software (Flater, 2005), for the "Plum Island, Merrimack River Entrance, Merrimack River, MA" station. Xtide uses the same tidal prediction algorithm as NOAA which results in a primarily 1.5 m amplitude (spring/neap average) semidiurnal tide, forced at the ocean boundaries, and includes 37 tidal constituents. A 5 cm/s ambient coastal current is applied on the northern boundary, flowing south. This has been considered representative of the Western Maine Coastal Current on this region in former simulations (Cole et al., 2020). The coastal current does not transport any stratification into the domain, as the typical deviations from ambient salinity measured in the current (~2 psu) are well offshore (>40 km; Geyer et al., 2004) and considered small relative to contributions from the Merrimack River.

SPICER ET AL. 4 of 21

The model is run for the months of April and May in 2019, with April used as the spin-up month and May as the analysis month. Typically, about 1 month is considered sufficient to spin up the Merrimack estuary, as it is a time-dependent salt wedge which reaches realistic estuarine conditions relatively quickly (Cole et al., 2020; Geyer et al., 2008; Ralston et al., 2010). April and May typically produce the largest river discharges of the year in the Merrimack, driven predominantly by locally increased rainfall but also by spring snowmelt from the White Mountains. It is during these months that the most energetic, defined tidal plumes form and so is the ideal timeframe for analysis. Winds are often elevated but variable in direction during these spring months (Fong et al., 1997), making the timeframe even more amiable for this study.

#### 2.2. Analysis

The analysis utilized in this work stems from the salinity variance equation, first introduced by Burchard and Rennau (2008) and further developed by Li et al. (2018). The relatively simple method links stratification, straining, and mixing in estuarine and coastal systems via deviations in salinity from volume and depth averages while allowing a time- and space-varying view of each term. As a basis, both vertical and horizontal deviations in salinity must be defined by choosing a control volume representative of the estuary or plume system. Generally, this volume should encompass the most active regions of straining and mixing in the system (Li et al., 2018). Within the control volume, we can state that  $S = \langle S \rangle + S'_{tot}$ , with S being the salinity at each 3-D coordinate,  $\langle S \rangle$  is the volume average of salinity, and  $S'_{tot}$  is the anomaly from the total volume average at each point. Decomposing salinity in the vertical direction gives a similar formulation:  $S = \overline{S} + S'_v$ , where  $\overline{S}$  is the depth average of salinity and  $S'_v$  is the deviation from the vertical average. Using the total and vertical deviations, we can calculate the corresponding horizontal deviation:  $S'_h = S'_{tot} - S'_v$ . By squaring each salinity deviation, we can represent the vertical salinity variance,  $(S_v')^2 = (S - \overline{S})^2$ , the horizontal variance,  $(S_h')^2 = (\overline{S} - \langle S \rangle)^2$ , and the total variance ance,  $\left(S_{tot}'\right)^2 = (S - \langle S \rangle)^2$ , at each 3-D coordinate (with the exception of  $\left(S_h'\right)^2$ , which does not vary with depth). Variance in this context is used as a metric for stratification, that is, vertical salinity variance physically represents vertical stratification of salinity and so these terms are used synonymously. Depth integrating each variance term gives the relationship:

$$\int (S'_{tot})^2 dz = \int (S'_h)^2 dz + \int (S'_v)^2 dz$$
 (1)

which then allows:

$$\int \int \int \left( S'_{tot} \right)^2 dx \, dy \, dz = \int \int \int \left( S'_h \right)^2 dx \, dy \, dz + \int \int \int \left( S'_v \right)^2 dx \, dy \, dz \tag{2}$$

where the left-hand side of Equation 2 represents the total variance in the control volume, while the right-hand terms represent the net horizontal and vertical variances (from left to right, respectively) in the volume.

For volume-integrated quantities, a semicircle with a 12 km radius originating at the river mouth is used to define the tidal plume control volume (Figure 1b). This volume includes the nearfield and midfield plume for all discharge events during the study period and omits the estuary, thereby enclosing the most active regions of plume mixing during a tidal pulse. As a check, the plume inertial radius ( $R_I = U/f$ , where U is the average plume velocity and f is the Coriolis frequency) is maximized near 12 km during the largest discharge events.  $R_I$  scales with plume spreading (Kakoulaki, 2015) and can be used as a simple metric to estimate the offshore extent of the combined near- and midfield plume. Generally, any portion of the plume which exceeds the 12 km radius is downcoast of the control region and is transitioning to the far-field plume, which mixes less intensely and evolves beyond a tidal time scale. Further, instantaneous wind effects have been considered negligible in their influence on Merrimack River plume dynamics beyond 12 km (Kakoulaki et al., 2014). By applying that region to Equation 2, we can determine bulk variance quantities over the control volume for the entire study period.

An important concept in the approached outlined by Li et al. (2018) is the ability for horizontal variance to be converted to vertical variance through straining. The crux of their solution is the derivation of the conservation of vertical salinity variance which allows for this transformation of (depth-integrated) variance:

SPICER ET AL. 5 of 21

wiley.com/doi/10.1029/2022JC018462, Wiley Online Library on [09/05/2023]. See the Terms

In Equation 3,  $\nabla_h$  is the horizontal gradient operator,  $u_h$  is the horizontal velocity vector,  $u_v'$  is the deviation of the 3-D velocity vector from a depth average ( $u = \overline{u} + u_v'$ ), and  $K_z$  is the vertical eddy diffusivity. In modeling studies such as this one,  $K_z$  is determined from the model turbulence closure (ranges from  $\sim 10^{-6}$  to  $\sim 10^{-2.5}$  m<sup>2</sup> s<sup>-2</sup> in these simulations). The terms in Equation 3 represent the net time rate of change of salinity variance, advection, straining, and dissipation/mixing (from left to right, respectively). Essentially, vertical salinity variance can be input to the system via advection (plume pulses from estuary) or created internally through straining (horizontal salinity gradients strain and create vertical salinity gradients). Vertical variance is destroyed by turbulent dissipation or transported out of the control volume by advection.

Conceptualizing what stratification (vertical variance) means in this work is important, as there are nuances in how many interpret stratification. In this context,  $\int (S'_v)^2 dz$  scales with the potential for vertical mixing to occur in the water column and does *not* quantify the strength of a density gradient. This means vertical variance and the terms comprising Equation 3 may vary according to water column depth, even if the density gradient of a stratified layer in the water column has an unchanged density gradient. This depth effect was found to be inconsequential to this analysis and is described in more detail in Appendix A.

#### 3. Results

#### 3.1. Environmental Conditions and Salinity Variance Variability

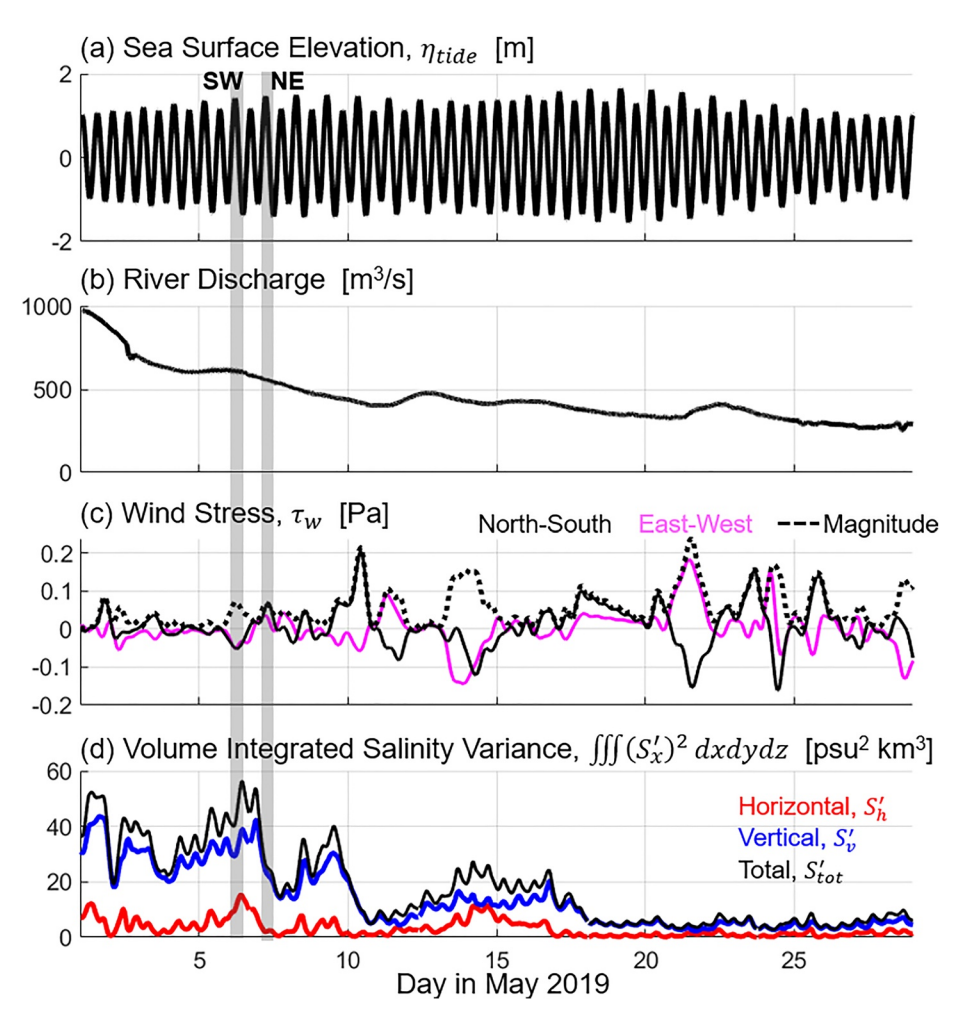
Typical spring-neap variability in sea surface elevation (Figure 2a) coupled with a steadily decreasing but significant river discharge (1,000 m³/s dropping to 300 m³/s in Figure 2b) created defined, energetic tidal plumes for the entire month of May 2019. Winds over the study period were particularly variable in magnitude and direction (Figure 2c), allowing an analysis which captured a wide spectrum of realistic wind forcing. Relatively larger magnitude wind events ( $\tau_w \sim 0.1$ –0.2 Pa [or  $\sim$ 8–11 m s<sup>-1</sup>]) were numerous and typically dominated by the north-south component, with a roughly even split between north or south dominance for those events. Enhanced east- or west-directed wind events were less prevalent. Typically, larger wind events (magnitude >0.1 Pa) lasted 24–48 hr, while moderate magnitude events ( $\sim$ 0.05 Pa [or  $\sim$ 5 m s<sup>-1</sup>]) lasted between 12 and 24 hr. Often rapid transitions (<12 hr between directional shifts) separated events. Light wind conditions (magnitude <0.05 Pa) occurred but were less frequent than the moderate conditions.

Figure 2d shows how the volume-integrated variance terms generally scale with discharge. That is, the largest variances in all components occur during the first 10 days of May, when river discharge exceeds 500 m³/s. Vertical variance accounted for most of the total variance at this time and varies between 20 and 40 psu² km³ while horizontal was much less at 5–10 psu² km³ (Figure 2d). Both vertical and horizontal variance are markedly smaller (<10 psu² km³) after day 10, when discharge drops below 500 m³/s. Similarly, tidal variability in all variance terms is more evident for the larger discharges (>500 m³/s) over the study period, with 12-hr ebb-flood oscillations in signal typically between 5 and 8 psu² km³ (before day 10, Figure 2d). For the smaller discharges, the intratidal differences are less than half that (2–4 psu² km³ after day 10, Figure 2d).

River discharge clearly dictates the overall mean trend (at scales of multiple days) in variance over the study period. Of second-order importance are winds, particularly the alongshore component, which create perturbations at a variety of time scales (days or less) to the mean variance set by discharge. At the Merrimack River mouth, winds in the north-south direction are aligned alongshore, whereas east-west is cross shore. The more noted reductions in total, vertical, and horizontal variance occur at roughly days 2, 3, 7, 10, and 17 and always follow, or coincide with, an alongshore wind stress directed north (in oceanographic convention, Figures 2c and 2d, hereby referred to as northward). Interestingly, the magnitude of the northward wind is seemingly unimportant in its ability to reduce variance, as both relatively larger (0.2 Pa, day 10) and moderate (0.08 Pa, day 7) northward wind events can reduce vertical variance by similar amounts (~25 psu² km³ for each). The disconnect between wind magnitude and vertical variance suggests that direct wind stress mixing is not of major importance to the destruction of stratification (discussed further in Section 3.3). Further, horizontal variance typically begins decreasing when vertical variance is maximizing during northward wind events (i.e., day 7), suggesting

SPICER ET AL. 6 of 21

2169291, 2022, 5, Downloaded from https://agupubs.onlinelibrary.wiley.com/doi/10.1029/2022/C018462, Wiley Online Library on [09/05/2023]. See the Terms and Conditions (https://onlinelibrary.wiley.com/derms-and-conditions) on Wiley Online Library for nules of use; OA articles are governed by the applicable Creative Commons License



**Figure 2.** (a) Sea surface elevation, (b) river discharge, and (c) wind stresses in oceanographic convention (east-west as magenta, north-south as solid black, and magnitude as dotted black) at the mouth of the Merrimack River for the month of May 2019. (d) Control volume-integrated vertical (blue), horizontal (red), and total (black) salinity variance is also shown for the month. Wind stress was low-pass filtered for 6 hr to smooth for this visual. The *x*-axis is the day of May 2019. The times over which plumes SW and NE from the analysis occur are shaded with gray boxes.

straining enhances vertical variance to some extent under northward winds. Vertical variance often continues to decrease for up to 12 hr following northward wind events, suggesting a plume-shelf condition is modified which is not directly wind driven (see days 1, 3, and 10, Figure 2). Further, large wind events in other directions (such as the strong southward wind event prior to day 15 in Figure 2c) have minimal influence on vertical variance (Figure 2d). During periods of gradually increasing variance (e.g., days 4–6 and 12–16) winds are either near zero or have a south-directed alongshore component (Figures 2c and 2d, hereby called southward). For the entire study period, the cross-shore wind stresses seem generally unassociated with decreases in vertical variance. In fact, vertical variance can increase under significant cross-shore wind forcing in either direction (i.e., west: days 6 and 7–9, or east: day 15, Figure 2d), indicating the cross-shore wind is less effective at clearing variance from the domain than the alongshore, particularly the northward component.

The Merrimack River plume has been found to be transported and sensitive to the alongshore component to wind, regardless if larger scale Ekman circulation patterns are or are not established, due to the plume's smaller spatial scales (Kakoulaki et al., 2014). The wind patterns identified in Figure 2 likely advect vertical variance in and out of the control volume in some accordance with the findings of Kakoulaki et al. (2014). To confirm the role of wind on advecting plume water, and to identify the more ambiguous roles of dissipation and straining in

SPICER ET AL. 7 of 21

controlling stratification under varying wind, we next decompose the spatial variability in dynamics between tidal plumes exposed to differing moderate wind conditions.

#### 3.2. Spatial Variability: Stratification

Two tidal pulses occurring roughly 24 hr apart from each other were analyzed to identify variability in plume dynamics between a wind blowing northeastward (hereby called plume "NE") and one blowing opposite, southwestward (called plume "SW," both labeled in Figure 2). NE and SW were chosen as they occur during similar tide and discharge conditions, have winds in opposing directions but same in magnitude, and are only 24 hr apart, allowing for relatively easy visualization of the transition from one plume to the next. Plume NE generally advects offshore, differing from the prototypical downcoast turning, coastal-trapped plume, which occur for most other winds conditions (like SW, discussed below). Analyzing plumes NE and SW therefore allows a relatively simple comparison between two dynamically different scenarios which occur within a day of each other.

During southwest winds (Figures 3a and 3b), the Merrimack River plume spreads out from the estuary and turns to the right. Surface currents are directed primarily to the right of the wind (toward west/northwest) and decrease in magnitude nearer to shore (Figure 3a), likely from an opposing barotropic pressure gradient created by both alongshore (downwelling favorable) and cross-shore (onshore) wind-driven sea level setup (Lentz & Fewings, 2012). The relatively weaker surface currents nearshore (x < 5 km) allow the plume to spread prototypically outward from the river mouth, but landward surface velocities in deeper water (x > 5 km) slow offshore propagation of the plume and Earth's rotation turns the plume downcoast (Figures 3a and 3e, respectively) in the direction of Kelvin wave propagation (i.e., anticyclonic). Enhanced vertical salinity variance over the shelf (log<sub>10</sub>  $(S'_n)^2 dz \sim 2.5 \text{ psu}^2 \text{ m}$  in Figure 3b) indicates that ambient coastal waters are stratified from former plumes not mixing or advecting out of the domain completely during the light wind conditions which occurred prior (Figure 2), allowing residual stratification to remain over the shelf. The remaining vertical variance then accumulates nearshore due to the landward surface currents. The new plume which pulses over the shelf adds to that stratification  $(\log_{10} \int (S_v^t)^2 dz \sim 3 \text{ psu}^2 \text{ m}$  in Figure 3b) as mixing again does not destroy all variance and surface flow promotes shoreward, anticyclonic plume advection, keeping the stratified water column trapped in the control volume. Horizontal variance is maximized at the river mouth where the plume begins spreading seaward (log 10  $\left(S_h'\right)^2 dz \sim 3 \text{ psu}^2 \text{ m}$ , Figure 3c) but is also enhanced downcoast of the mouth  $\left(\log_{10} \left(S_h'\right)^2 dz \sim 2-2.5 \text{ psu}^2 \text{ m}\right)$ , Figure 3c) in the region of shore-trapped vertical variance. Horizontal variance remains elevated and does not exhibit significant variability over the tidal pulse.

The role of advection in steering plume and ambient shelf water clearly differs during the opposing northeast wind case as the plume advects mainly offshore (Figure 3d). Surface currents are mainly directed with the wind (toward northeast) or to the right of it (east) and are similar in magnitude both nearshore (x < 5 km) and in deeper water. Unlike plume SW, the offshore and upwelling-favorable wind components likely prevent an opposing barotropic flow (Figure 3d). The plume advects offshore more readily, exhibiting a sensitivity to the shelf's surface current wind response (Figure 3h; similar to findings in Kakoulaki et al. [2014]). Consequently, residual vertical variance over the shelf from former tidal pulses (the light then SW winds) is pushed offshore with the new plume (Figure 3e). This advection of vertical variance out of the control volume results in a nearly homogenous water column over the inner shelf in the vicinity of the nearfield river plume (<5 km from shore,  $\log_{10} \int (S'_v)^2 dz \sim 0.5$  psu<sup>2</sup> m in Figure 3e). During plume NE, horizontal variance is again maximized at the river mouth ( $\log_{10} \int (S'_v)^2 dz \sim 3$  psu<sup>2</sup> m in Figure 3e) but is notably diminished in the remainder of the control volume relative to SW, suggesting straining may be more active in converting horizontal variance to vertical under northward winds.

Former work in the Merrimack found the plume to generally follow the direction of wind, regardless of duration, due to the short time and spatial scales over which it exists on the shelf (Kakoulaki et al., 2014), and supports the advection trends outlined here. Here, we see a similar sensitivity of the ambient stratification to wind direction. Although we hypothesize that straining is modulated by wind direction, it remains unclear, as is the wind effect on the mixing of variance. We next analyze the spatial structure of straining and dissipation for plumes SW and NE to identify where each term is most dominant spatially and what that implies in the context of plume dynamics.

SPICER ET AL. 8 of 21

21699291, 2022, 5, Downloaded from https://agupubs. onlinelibrary.wiley.com/doi/10.1029/2022/C018462, Wiley Online Library on [09/05/2023]. See the Terms and Conditions (https://onlinelibrary.wiley.com/terms-and-conditions) on Wiley Online Library for rules of use; OA articles are governed by the applicable Creative C.

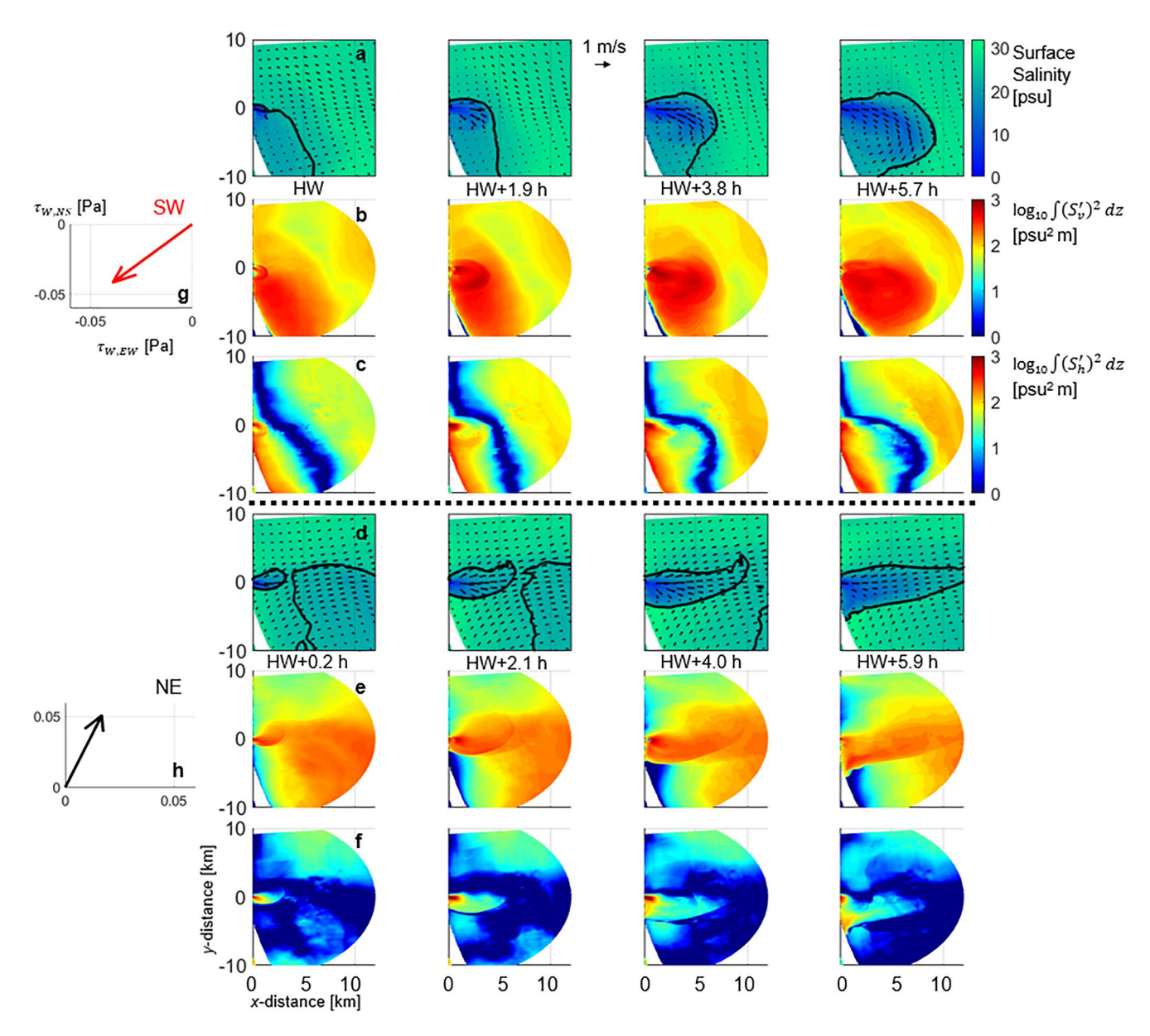


**Figure 3.** Snapshots of plume SW (a–c) and NE (d–f) over a tidal pulse. Surface salinity contours are shown for each case with the 23 psu isohaline given as a solid line and surface current vectors as black arrows (a, d) as well as the depth-integrated vertical salinity variance (b, e) and horizonal salinity variance (c, f) on a log<sub>10</sub> scale. Each plume is depicted over a roughly 6-hr tidal pulse, with times in reference to high water (HW) shown (a, d). Mean wind stresses (with north-south [NS] and east-west [EW] components) over each plume are given as vectors (g, h). Horizontal axes are the *x*-distance and vertical are *y*-distance.

#### 3.3. Spatial Variability: Mixing and Straining

For plume SW, the nearfield region (<5 km from mouth) dominates straining for the entire tidal pulse  $(\int -2u'_vS'_v \cdot \nabla \overline{S} \, dz > 0.1 \text{ psu}^2 \text{ m s}^{-1}$ , Figure 4a) as the estuarine outflow shoals, thins, and spreads over saltier receiving waters, converting horizontal variance to vertical. The frontal region can be identified in each snapshot as the band of relatively intense negative straining  $(\int -2u'_vS'_v \cdot \nabla \overline{S} \, dz = -0.01 \text{ to } -0.1 \text{ psu}^2 \text{ m s}^{-1}$ , Figure 4a) which propagates outward from the river mouth over the tidal pulse. Negative straining occurs near the plume front because horizontal variance is added to the shelf as the plume front passes. Between the front and nearfield plume, straining is generally positive but smaller in magnitude (often by an order of magnitude or more) than the nearfield  $(\int -2u'_vS'_v \cdot \nabla \overline{S} \, dz \sim 0.01 \text{ psu}^2 \text{ m s}^{-1}$ , Figure 4a). Dissipation of vertical variance in the nearfield dominates relative to the remainder of the plume footprint (<5 km from mouth,  $\int -2u'_vS'_v \cdot \nabla \overline{S} \, dz > 0.1 \text{ psu}^2 \text{ m s}^{-1}$ ,

SPICER ET AL. 9 of 21

21699291, 2022, 5, Downloaded from https://agupubs.onlinelibrary.wiley.com/doi/10.1029/2022/C018462, Wiley Online Library on [09/05/2023]. See the Terms and Conditions (https://onlinelibrary.wiley.com/terms

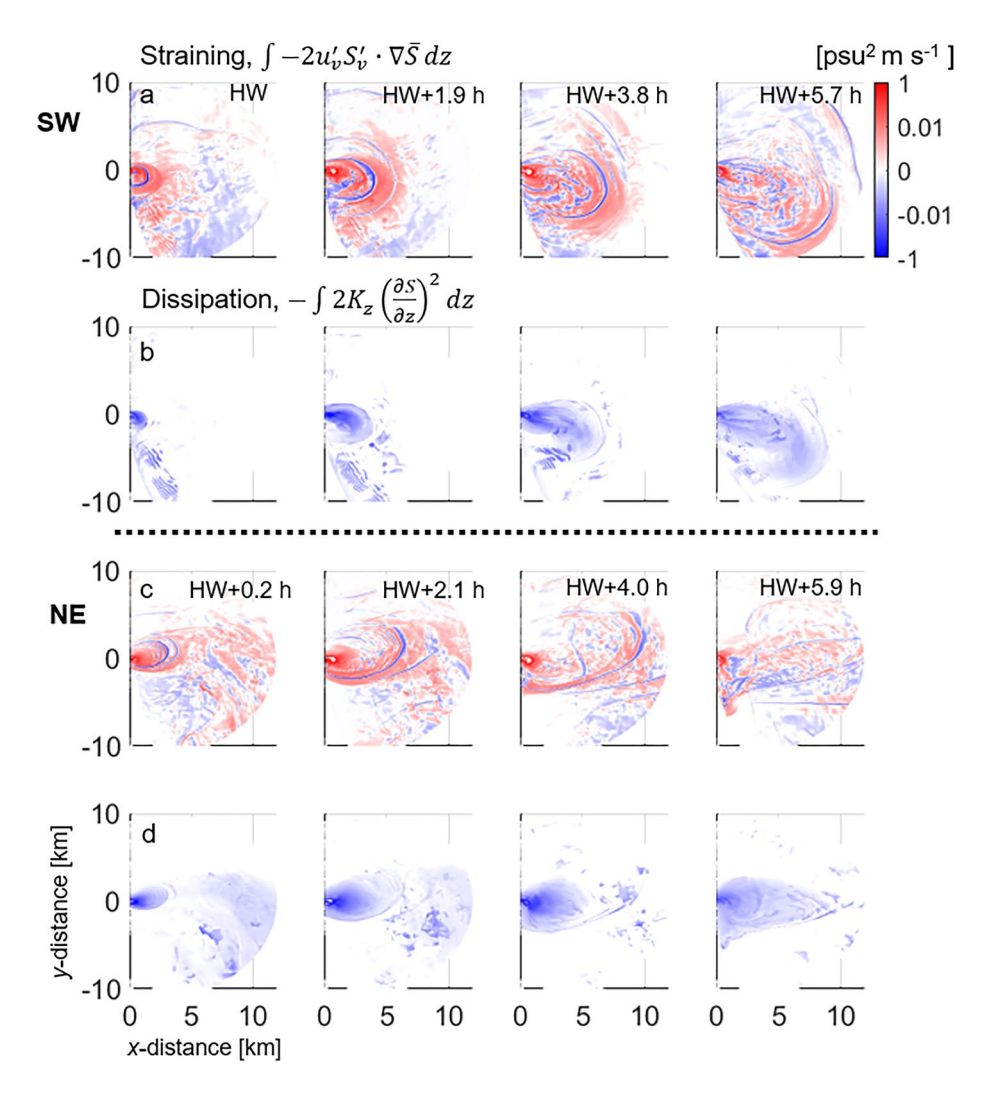


**Figure 4.** Plan view snapshots of straining (a, c) and dissipation of vertical variance (b, d) on a  $\log_{10}$  scale for plumes SW (a, b) and NE (c, d). Time steps match those from Figure 3. Horizonal axes are the *x*-distance and vertical are *y*-distance.

Figure 4b). Dissipation decreases significantly beyond the nearfield and is at least an order of magnitude less in most of the plume interior (>5 km from mouth,  $\int -2u'_v S'_v \cdot \nabla \overline{S} \, dz \sim 0.01 \, \mathrm{psu}^2 \, \mathrm{m \ s^{-1}}$ , Figure 4b). For plume NE, patterns in straining and dissipation are largely the same, that is, the nearfield dominates regardless of wind direction (Figures 4c and 4d). For both plumes, SW and NE dissipation is largely near 0 outside the plume foot print, suggesting that direct surface wind mixing is likely of secondary importance to stratified shear mixing during moderate wind events, as has been hypothesized in former work (Horner-Devine et al., 2015). Intense mixing on the shelf of a similar scale to that occurring within the plume would indicate direct wind mixing to be a more important dynamic.

Straining and dissipation dominate in the nearfield plume, regardless of wind, but it is difficult to identify variability in the terms between the river mouth and front. To better quantify spatial variability in the terms, a salinity coordinate approach was utilized (Hetland, 2005). Salinity coordinates are useful as they translate with the plume as it progresses over an ebb pulse. Differences in dynamics between plume regions can be isolated and identified more easily when comparing regions of similar salinity versus static locations. The coordinates here are based on surface salinities, as they are broadly representative of plume-layer salinities and easily compared to Figure 3. To further bridge spatial and salinity coordinates, we quantified the average surface salinity of radial bands (in 1 km increments) moving from river mouth to 12 km offshore (Figure 5a). For both plumes SW and NE, average salinity increases moving offshore from the mouth and becomes fresher with time as each plume expands. Average salinity for all time steps in both plumes converge at the ambient shelf salinity, ranging from 23 to 26 psu

SPICER ET AL. 10 of 21

21699291, 2022, 5, Downloaded from https://agupubs.onlinelibrary.wiley.com/doi/10.1029/2022IC018462, Wiley Online Library on [09/05/2023]. See the Terms and Conditions (https://onlinelibrary.wiley

articles are governed by the applicable Creative Commons License

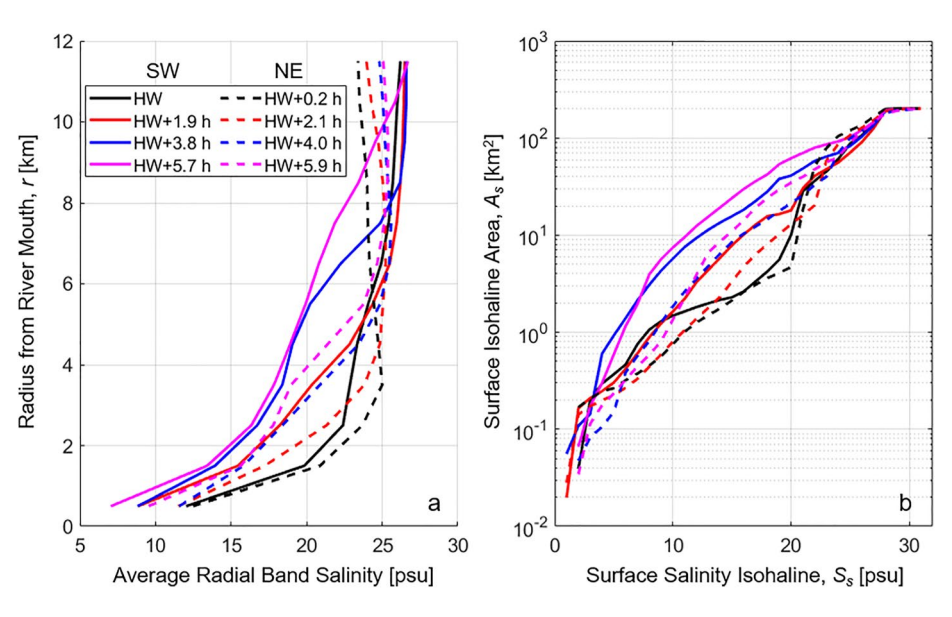


Figure 5. (a) Average salinity (x-axis) per 1 km radial bands (y-axis) moving from river mouth (r = 1 km) to edge of control volume (r = 12 km), and (b) area (y-axis) enclosed by each surface salinity contour (x-axis) at four similar times (relative to high water [HW]) during plume SW (solid lines) and plume NE (dashed lines). Time steps match those from Figures 3 and 4.

(Figure 5a). Plume NE features a relatively defined location where time steps converge ( $r \sim 6$  km, Figure 5a), indicating the average ambient surface salinity is near 25 psu. Plume SW shows significantly more salinity variation in the r = 5-10 km range, with no obvious convergence point between time steps, demonstrating the ambient shelf salinity is more variable and likely falls between 22 and 26 psu depending on location (Figure 5a, also shown in Figure 3).

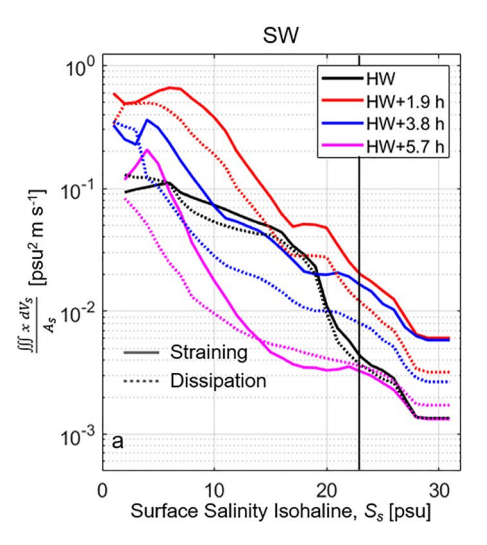
Transitioning to salinity coordinates, in general, there are larger spatial regions of the 5–23 psu surface salinity class in plume SW relative to plume NE, which persist over the entire tidal pulse (Figure 5b). A rough comparison to Figures 3a and 3c indicates that the 0–10 psu class roughly corresponds to the nearfield plume (minimal rotation downcoast), while 10–23 psu matches the midfield plume (remainder of plume area). Some ambient shelf water from residual stratification falls in the 20–23 psu range and thereby skews isohaline areas up in that range (Figure 3a). Size discrepancies between SW and NE below 20–23 psu, in the near- and midfield plume, are not skewed by shelf salinity and indicate that variability in straining and dissipation exists in those regions.

The intensity of vertical variance dissipation, along with straining, was quantified following salinity coordinates to determine variability. Here, we consider intensity to be the volume integral of either dissipation or straining (magnitude), divided by the area over which it acts:  $\int \int x \, dV_s / A_s$ , with x representing absolute values of either straining  $(|2u_v'S_v' \cdot \nabla \overline{S}|)$  or dissipation  $(|2K_z(\partial S/\partial z)^2|)$ , and  $V_s$  being the volume beneath the area,  $A_s$ , enclosed by isohaline, s (area from Figure 5), which extends vertically to the seabed. A larger intensity in either term indicates more dissipation and/or straining per unit area. For all plume regions enclosed by the ~23 psu salinity class or less, both straining and dissipation are generally more intense in plume NE (Figure 6). Using the 10 psu isohaline as example, during midpulse (~4 hr after high water, blue lines in Figure 6), dissipation intensity is nearly 1 order of magnitude larger in the plume exposed to NE winds than SW (Figure 6). Differences between each plume are much less noted beyond the 23 psu isohaline, confirming the lessening importance of dissipation and straining processes moving away from the nearfield into the midfield and ambient shelf (Figure 6). Collectively, the relative area of the near- and midfield plume for plume NE is less than that of SW but dissipation and straining are significantly more important.

SPICER ET AL.

21699291, 2022, 5, Downloaded from https://agupubs.onlinelibrary.wiley.com/doi/10.1029/2022JC018462, Wiley Online Library on [09/05/2023]. See the Terms and Conditions

onditions) on Wiley Online Library for rules of use; OA articles are governed by the applicable Creative Commons Licens



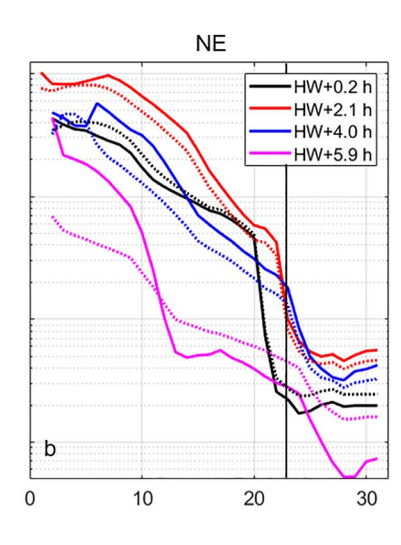


Figure 6. Intensity (y-axis) of straining  $\left(x = \left| 2u'_v S'_v \cdot \nabla \overline{S} \right| \right)$  and dissipation of vertical variance  $\left(x = \left| 2K_z (\partial S/\partial z)^2 \right| \right)$  for a given region bounded by each surface isohaline (x-axis) at similar times (relative to high water [HW]) for plume SW (a) and plume NE (b). Intensity is determined by taking the volume integral of x over the region  $A_s$ , then dividing by  $A_s$ . Straining is shown as solid lines while dissipation is dotted. The 23 psu isohaline is marked with a vertical black line. Time steps match those from Figures 3–5.

#### 3.4. Mixing and Straining Mechanisms in the Nearfield Plume

In comparing two tidal plumes created by similar river discharges, we have shown that moderate wind stresses opposing the direction of Kelvin wave propagation can alter the dynamics of the Merrimack River plume-shelf system, notably by advecting vertical variance offshore, thereby homogenizing the water column nearshore, and increasing straining and dissipation of vertical variance in the near- to midfield river plume. We now investigate the physical mechanisms which lead to dissipation and straining to connect the terms to wind direction, the ambient shelf condition, and the strength of the nearfield plume density gradient (which is not directly quantified via  $(S'_{\nu})^{2}$ ).

Time- and depth-varying salinity and currents at a nearfield plume location (x = 1 km, y = -1 km from the river mouth) portray changes in hydrography as winds transition from SW to NE (Figure 7). Former research in the Merrimack indicates that 1 km from the river mouth is always part of the nearfield tidal plume (Hetland & MacDonald, 2008; MacDonald et al., 2007). When the wind change occurs (roughly day 6.7 in Figure 7) successive plumes become thinner than SW (see dashed line approach surface, Figure 7a). Although thinner, surface waters in NE are just as fresh as SW (~10 psu, Figure 7a) and offshore advection of variance creates a saltier ambient shelf condition beneath NE (30 psu isohaline moves toward surface over time, Figure 7a), creating a stronger density gradient at the plume base. Further, winds during plume NE enhance offshore-directed (east) ebb current velocities within the thinned plume (u increases from 0.5 to 0.8 m s<sup>-1</sup>, Figure 7c), subsequently increasing shear in the nearfield of NE relative to SW. Increased offshore transport in the plume is likely due to wind augmenting ebb tide and discharge momentum. A recent study in the Fraser River plume supports this: winds opposing Kelvin wave propagation created a faster moving, offshore-advected plume, whereas winds in the opposite direction created a "typical," slower, onshore rotating plume (Kastner et al., 2018). These wind-induced increases in shear likely create the enhanced straining observed in the near- and midfield plume (as quantified in Figure 6b) which thin the plume, as described here. Wind-enhanced straining has been observed similarly in estuaries, where winds blowing in the same direction as surface currents increase shear in the water column (Scully et al., 2005).

We next link the salinity variance method to classic turbulence theory at the same nearfield plume location (x = 1 km, y = -1 km) to identify how wind straining of plume NE over a saltier shelf can modulate mixing. Mixing is expected in the nearfield during most tidal pulses due to intense shear overcoming stratification and creating vertical instabilities. We can verify mixing conditions are likely when the gradient Richardson number,

SPICER ET AL. 12 of 21

21699291, 2022, 5, Downloaded from https://agupubs.onlinelibrary.wiley.com/doi/10.1029/2022JC018462, Wiley Online Library on [09/05/2023]. See the Terms and Conditions (https://onlinelibrary.wiley.com

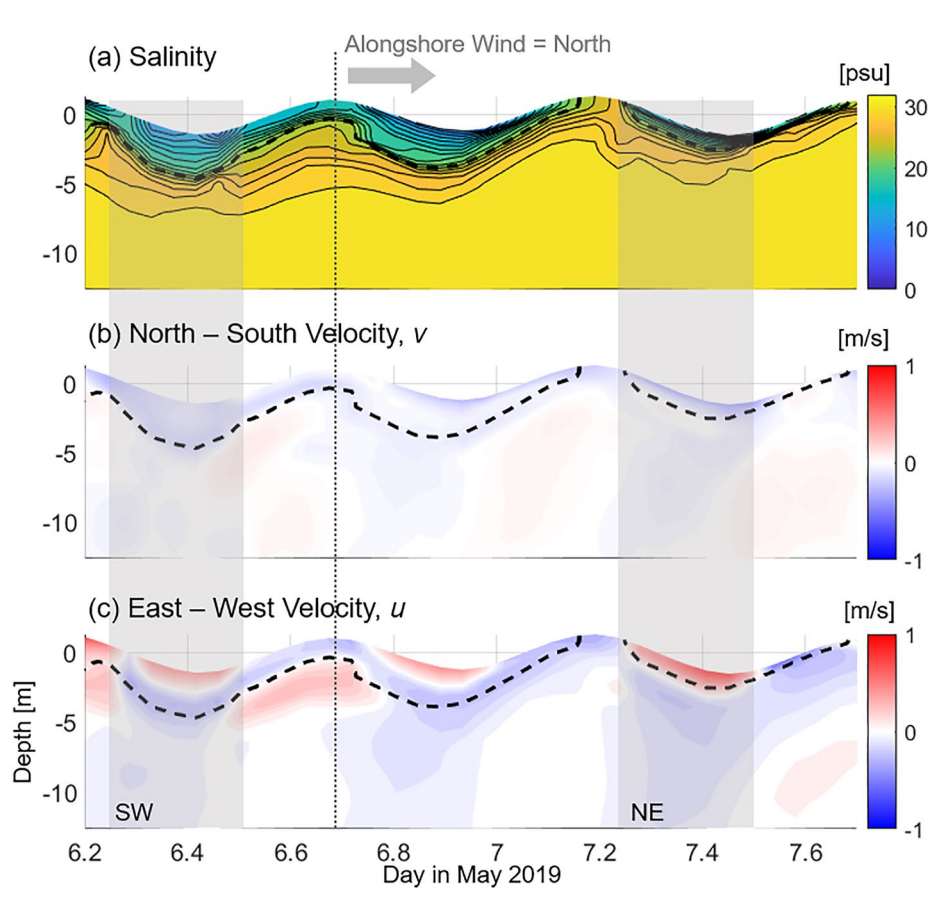


Figure 7. (a) Salinity, (b) north-south velocity, and (c) east-west velocity at a nearfield plume location (x = 1 km, y = -1 km) during days 6 and 7 of May 2019 (x-axis). Plumes SW and NE are outlined with gray boxes and labeled. The 23 psu isohaline is marked with a dashed line. Contours in (a) mark every other isohaline between 32 and 0 psu. The point where winds shift toward the north is marked with a dotted gray line and labeled. The y-axes are water depth.

 $Ri = N^2/S^2$  (where  $N^2$  is the buoyancy frequency and  $S^2$  is the squared vertical shear in horizontal currents), is at a critical value of 0.25 or less. During both SW and NE, Ri holds at or below the threshold, indicating mixing should occur for both plume (Figure 8a). Shear production,  $P = -\overline{u'w'} \left( \frac{\partial u}{\partial z} \right) - \overline{v'w'} \left( \frac{\partial v}{\partial z} \right)$  (where  $\overline{u'w'}$  and  $\overline{v'w'}$ are the Reynold's stresses in the x and y directions, respectively, with primes indicating fluctuating quantities and overbars ensemble averages), quantifies the production of turbulence by the interaction of mean shear and Reynold's stresses (from the turbulent kinetic energy [TKE] equation). Conceptually, P is the result of eddies being strained by mean shear and is a source term which is always positive (Monismith, 2010). The magnitude of P is elevated in the wind-strained NE plume ( $10^{-4}$  m<sup>2</sup> s<sup>-3</sup>, Figure 8b) relative to SW ( $10^{-4.5}$  m<sup>2</sup> s<sup>-3</sup>, Figure 8b). The elevated P acts directly on the stronger density gradient at the base of plume NE, whereas it is confined within the plume layer of SW (Figure 8b). Shear production is then compared to the turbulent buoyancy flux,  $B = \frac{g}{\rho' w'}$  (where  $\rho_0$  is a reference density and  $\rho' w'$  are the Reynolds fluxes), to identify how elevated P acting on a more intense density gradient at the plume base translates to mixing. In these simulations (no convection), B represents a consumption (sink) of TKE (produced by P) by buoyancy forces which physically results in the mixing of buoyancy (Monismith, 2010). Like P, buoyancy flux at the plume base is larger in magnitude during NE  $(10^{-5} \text{ m}^2 \text{ s}^{-3}, \text{ Figure 8c})$  relative to SW  $(10^{-5.5} \text{ m}^2 \text{ s}^{-3}, \text{ Figure 8c})$ . The depth-averaged B is similar for both plumes (10<sup>-5.5</sup> m<sup>2</sup> s<sup>-3</sup>, Figure 8d), indicating mixing in the plume layer becomes more concentrated, or intense, at the interface of the thinned NE plume. The dissipation of variance term, being sensitive to both  $K_z$  (increases with P) and  $\partial S/\partial z$  (increases from advection of stratification offshore), maximizes during NE (Figure 8d). Figure 8 suggests that larger shear production likely occurs from wind straining and acts on a larger density gradient at the plume base (created from wind straining thinning the plume and advection setting up saltier water beneath) subsequently allowing the local dissipation of vertical variance to maximize.

SPICER ET AL. 13 of 21

21699291, 2022. 5, Downloaded from https://agupubs.onlinelibrary.wiley.com/doi/10.1029/2022/C018462, Wiley Online Library on [09/05/2023]. See the Terms and Conditions (https://onlinelibrary.wiley.com/rerms/com/rerms

and-conditions) on Wiley Online Library for rules of use; OA articles are governed by the applicable Creative Commons Licenso

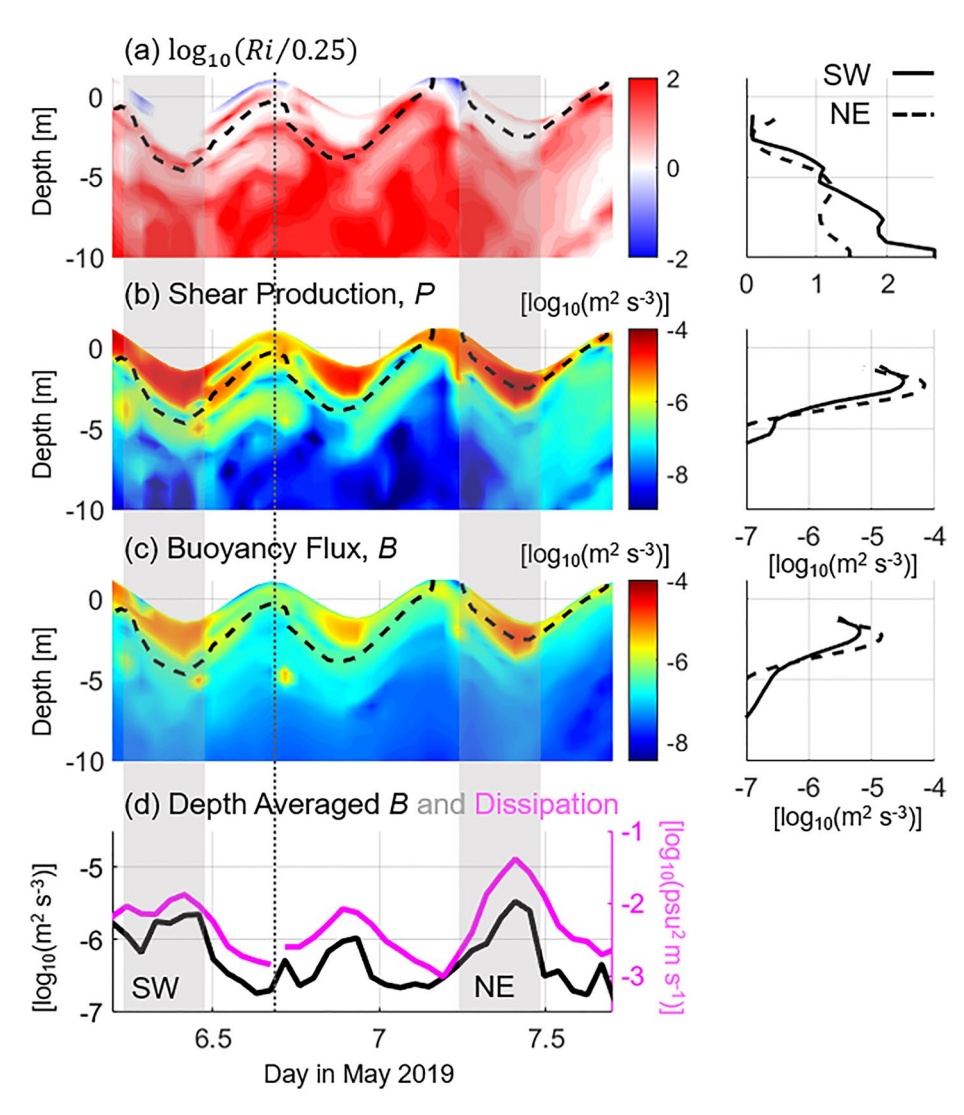


**Figure 8.** Filled contours of (a) Richardson number divided by 0.25, (b) turbulent shear production, P, and (c) turbulent buoyancy flux, B, at a nearfield plume location (x = 1 km, y = -1 km) during days 6 and 7 of May 2019 (x-axis). Right panel line plots give profiles at low water during plume SW (solid) and NE (dashed). Line plots (d) of depth-averaged B (black) and dissipation,  $\int 2K_z(\partial S/\partial z)^2 dz$  (magenta). All data are subsampled to hourly resolution. Color bars (a–c) and y-axes (d) are on a  $\log_{10}$  scale. Plumes SW and NE are outlined with gray boxes and labeled. The 23 psu isohaline is marked with a dashed line. The point where winds shift toward the north is marked with a dotted gray line. The y-axes in (a)–(c) are water depth.

#### 3.5. Major Trends and Relative Importance of Mixing to Straining

We now expand these findings to the remainder of the tidal plumes in the study period and identify exceptional cases. The terms in the conservation of vertical variance equation (Equation 3) were evaluated and averaged over the control volume for the entire month (Figure 9). As established in Figure 4, the nearfield and midfield plume dominate overall dissipation and straining in the control volume, so general variability shown in Figure 9 can be considered controlled by those plume regions with negligible influence from the ambient shelf. Straining is largely balanced by dissipation, which is opposite in sign but often smaller in amplitude, particularly for larger river discharges in the beginning of the month (Figure 9b). The excess variance which is not destroyed by dissipation is generally accounted for via advection (Figure 9b). At subtidal scales (30 hr low-pass-filtered terms, Figure 9c), advection and the net time rate of change of vertical variance are nearly identical, and so similar to Li et al. (2018) we regard them as one in the same. Negative advection therefore indicates transport of excess stratification out of the domain, while positive indicates an accumulation of stratification within the domain. Residual stratification remaining in the domain and that which is immediately advected out will ultimately contribute to

SPICER ET AL. 14 of 21

21699291, 2022, 5, Downloaded from https://agupubs.onlinelibrary.wiley.com/doi/10.1029/2022IC018462, Wiley Online Library on [09/05/2023]. See the Terms and Conditions (https://onlinelibrary.wile

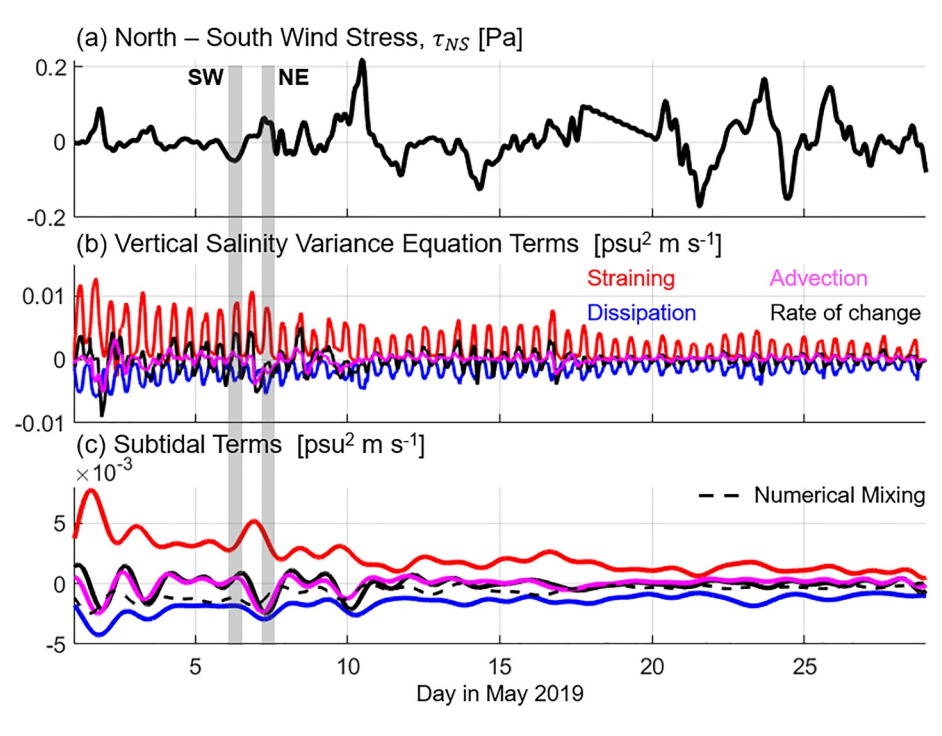


**Figure 9.** (a) North-south wind stress, (b) area-averaged vertically integrated salinity variance equation terms (straining in red, dissipation in blue, advection in magenta, and net rate of change in black), and (c) the 30-hr low-pass-filtered (subtidal) version of panel (a) with numerical mixing added (dashed black). The *x*-axis is the day of May 2019. The times over which plumes SW and NE from the analysis occur are shaded with gray boxes.

the far-field plume and persist at time scales longer than tidal. The northward wind events identified as strong destratifying events (e.g., days 2, 3, 7, 10, and 17 in Figure 9a) nearly always result in transport of stratification out of the domain (negative advection, Figures 9b and 9c) due to offshore and/or upcoast (opposing Kelvin wave) surface currents which counter the anticyclonic tendency of the plume. Most plumes exposed to northward winds are also generally accompanied by enhanced straining and dissipation of variance (Figure 9), confirming analysis in prior sections. Interestingly, the greatest dissipation enhancement from northward winds tends to also occur on the tide immediately following the negative advection (northward wind) event (Figure 9b). Maximum straining does not lag advection, indicating the northward winds have an immediate effect on advection and straining, as expected, but maximum dissipations seem more prone to occur after the ambient shelf is cleared of residual stratification following a wind event.

It has been determined that northward winds enhance negative advection, plume straining, and dissipation of variance, while dissipation can remain elevated following north wind events. It remains unclear if dissipation is more effective at eliminating vertical variance created by straining during or after the north wind events relative to typical conditions. We quantified the ratio of dissipation to straining for every tidal plume in the month of May 2019 to investigate. We found the plume dissipation–straining ratio is most connected to the initial ambient shelf stratification prior to a tidal pulse (high water) which in turn is linked to the average wind from the previous 12 hr. The initial shelf stratification, quantified as a volume integral of vertical variance  $\left(\int \int \left(S'_{v}\right)^{2} dx \, dy \, dz\right)$ outside the estuary prior to each plume in May 2019, is smallest typically following wind events with a northward component and negative net advection when stratification is pushed offshore and out of the control volume (north mean = 10.5 psu<sup>2</sup> km<sup>3</sup>, south mean = 15.8 psu<sup>2</sup> km<sup>3</sup>, Figure 10a). A few notable southward wind events also result in diminished variance on the shelf, but these events are the minority relative to winds aimed north (Figure 10a). The tidal plumes which develop after the northward, negative advection events then tend to have the largest ratio of dissipation to straining, with both terms volume and time integrated over the tidal pulse (Figure 10b). A dissipation-straining ratio greater than 1 in this context indicates that more vertical variance is diminished over a 12 hr tide than internally produced (vertical variance input via advection can be destroyed as well, thus allowing the ratio to exceed 1), whereas the same ratio less than 1 means not all the stratification

SPICER ET AL. 15 of 21

21699291, 2022, 5, Downloaded from https://agupubs.onlin

elibrary.wiley.com/doi/10.1029/2022JC018462, Wiley Online Library on [09/05/2023]. See the Terms

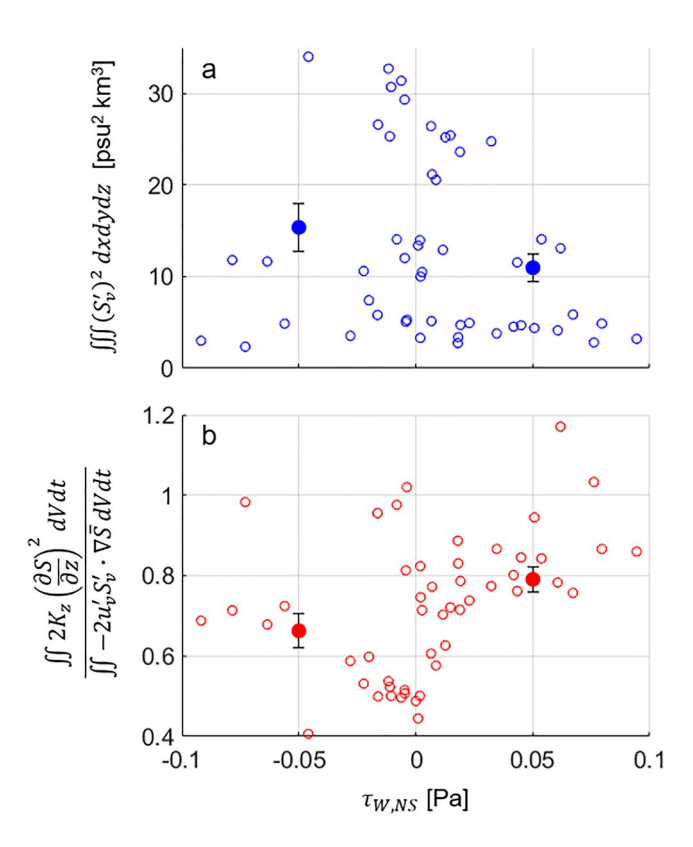


**Figure 10.** (a) Preebb pulse volume-integrated vertical salinity variance on the shelf (*y*-axis) versus the average north-south wind stress over the 12 hr prior to each plume (*x*-axis), with positive indicating a wind blowing north, for every tidal plume in the month off May 2019 (dot = different plume). (b) Volume- and time-integrated ratios of dissipation to straining over each ebb pulse (*y*-axis) versus north-south wind stress. Scattered values on each plot are averaged by wind direction (south or north) and given as the large, filled dots with standard error bars.

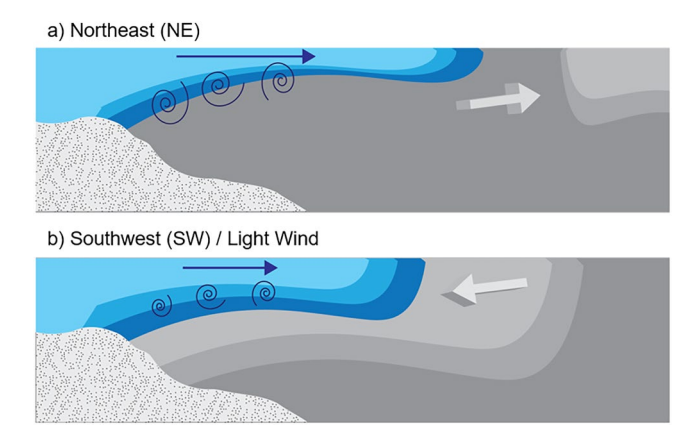


**Figure 11.** Conceptual diagram showing when mixing in the nearfield of a tidal plume can increase due to wind effects. Blue and gray contours represent water of similar density. Light blue is the freshest plume water, whereas dark gray is the saltiest ambient water. Blue arrows scale with plume velocity magnitude and white 3-D arrows point in the direction which winds and surface shelf waters are moving. Mixing intensity scales with the dark blue swirls. Scenarios depict (a) northeastward (NE) and (b) southwestward (SW)/ light wind scenario.

produced from straining on a tidal pulse is destroyed over the tidal pulse. The largest ratios (>0.75) are predominately produced after northward wind events (north wind mean = 0.8), with only a few exceptional south wind events producing similar ratios (south wind mean = 0.65, Figure 10b). Figure 10 therefore provides two main insights: (a) stratification produced by straining (dominated by the nearfield plume) is most effectively mixed away by dissipation following north wind events when dissipation is enhanced but straining is no longer wind enhanced, and (b) dissipation–straining ratios during south or light wind scenarios are generally less than 0.75, indicating more excess vertical variance is created which persists beyond a tidal pulse (ranging from 20% to 60%).

#### 4. Discussion

Winds which initiate surface currents opposing the direction of Kelvin wave propagation on the shelf tend to decrease net stratification over the control volume most effectively (Figure 2). After analysis of two tidal plumes under varying winds and all plumes in the full month of May 2019, we attribute the decrease in net stratification to advection of ambient stratification offshore and a subsequent increase in stratified shear mixing in the near- and midfield river plume from wind straining and intensified density gradients at the plume base (Figure 11a). Conversely, winds creating surface currents aimed in the direction of Kelvin wave propagation or weak in magnitude advect the plume and ambient shelf variance nearshore, decrease wind straining relative to the former case, and create a less intense density gradient at the plume base which subsequently leads to less intense mixing (Figure 11b). Dissipation of variance was found to remain enhanced following wind events, as long as the ambient shelf is clear of "old" plume stratification.

# **4.1.** Tidal Time Scale Wind Transport Effects in the Merrimack and Beyond

This work describes when mixing of a tidal plume may be enhanced under certain winds. Past research investigating wind effects on plumes has primarily identified the far-field region as being prone to modification from wind (e.g., Fong & Geyer, 2001; Hetland, 2005; Lentz, 2004). This study confirms the hypothesis of Kakoulaki et al. (2014): wind can in fact modify nearfield mixing in tidal plumes and expands on the work of Kastner et al. (2018), who first identified differing nearfield mixing rates from winds. Here, we find it valuable to place this work within the context of the Merrimack study by Kakoulaki et al. (2014), Fraser plume work of Kastner et al. (2018) and others to intercompare and extrapolate these results elsewhere.

A major concept presented in this study is the relatively quick response of both the plume and shelf waters to wind stresses. The advection of plume and shelf stratification offshore, and subsequent replenishment of the near-coast shelf with salty water during northward wind events can occur on a tidal time scale, much more quickly than what typical upwelling-driven Ekman transport would dictate (subtidal). This aligns with results from Kakoulaki et al. (2014) who found instantaneous winds to generally dictate advection in the Merrimack plume when above a 4 m s<sup>-1</sup> threshold (similar to the  $\sim$ 0.05 Pa wind stress seen here) and within a 12 km offshore distance from the river mouth, as those winds create surface currents on the order of the barotropic tidally

SPICER ET AL. 16 of 21

produced plume velocities with relatively fast adjustment times. Winds less than that allow rotation and plume discharge to dominate transport, and the authors speculate larger scale circulation patterns would gain influence in deeper water beyond the midfield plume, or nearshore if winds sustain direction and magnitude at subtidal time scales. Because the Merrimack plume and winds evolve mainly at tidal time scales, the plume is not influenced in a meaningful way by Ekman processes which typically develop under steady wind forcing over multiple days in midlatitude regions (Kämpf, 2017). Further, the relatively shallower shelf over which the Merrimack plume spreads ( $\sim$ 50 m maximum) is mainly considered a "shallow water region" where interference occurs between the bottom and surface Ekman layers (typically layers are  $\sim$ 45 m deep at midlatitudes with a 5 m s<sup>-1</sup> wind), effectively shutting down Ekman circulation (unlike plumes which discharge over the deeper Pacific shelves e.g.) and aligning plume and ambient shelf surface currents with the instantaneous wind (Kämpf, 2015, 2017; shown in Figure 3). Therefore, the direct enhancement or diminishment of velocities in the interior plume during wind events in this study (mainly over 4 m s<sup>-1</sup>, not shown) was considered a significant control on near- and midfield straining and dissipation of variance and builds on the work of Kakoulaki et al. (2014).

In the Fraser River plume, Kastner et al. (2018) observed a plume relatively sensitive to wind which dynamically changed depending on whether wind opposed or supported Coriolis in the plume momentum balance. For opposing winds, faster plume currents are produced, and transport is offshore directed (like in the Merrimack). When winds support the Coriolis force, the plume rotates shoreward relatively more slowly (also like the Merrimack). The findings of Kastner et al. (2018) aid this research in explaining the dynamical behavior of plume transport and velocities under differing winds. We augment the results of Kastner et al. (2018) by connecting wind to straining and advection-driven modulation of interior plume variance dissipation, building on and perhaps explaining the mixing trends observed in their work. Although net mixing was larger in the offshore-advecting Fraser plume, intensity in the nearfield was not relative to their typical case. Further, the offshore-advected Fraser is thicker than the downcoast turning case, opposite of these Merrimack simulations. It is likely that the deep, tidally flushed Strait of Georgia which controls ambient stratification flushes variance from the river mouth more effectively than at the Merrimack, regardless of wind. Mixing dynamics would therefore rely more on plume geometry (as outlined in Kastner et al. [2018]) and likely the straining discussed in this work rather than the more indirect ambient shelf stratification effects also introduced here. Additionally, the significant ebb currents working in concert with wind in the offshore-advected Fraser case likely means shear at the plume base is less intense than the downcoast turning plume: that is, tidal currents at depth opposing surface flow increase shear (Merrimack, see east-west velocities, Figure 7c) while tidal currents moving in the same direction as the plume layer likely result in less intense shear at the plume base (Fraser).

In the much larger Columbia River plume, winds gain influence on plume dynamics mainly after Ekman dynamics are established (Hickey et al., 1998, 2010). These upwelling/downwelling subtidal circulations are typical over the deep shelf in the region of the Columbia mouth, and stronger than what would be expected in the shallower regions near the Merrimack River mouth. It is likely the findings presented in this work would not apply in the Columbia, as subtidal wind effects are presumably of more importance. That said, results from this study should be extendable to other small- to medium-sized tidally pulsed plumes over shallow shelves.

#### 4.2. Limitations and Future Work

Application of the salinity variance equation via numerical methods was particularly amiable in investigating this topic, as real-life conditions often make sampling river plumes in moderate to heavy winds difficult to impossible. That said, there are a few limitations to this research which are worth addressing.

Waves were not modeled in these simulations. Former work has identified breaking waves can have a substantial impact on plume structure and some dynamics, but likely not modify mixing with ambient waters in a meaningful way (Gerbi et al., 2013; Kastner et al., 2018). That said, wave action could impact mixing of the residual stratification from former plumes and modify the ambient shelf condition (Gerbi et al., 2015). Further, mixing in the plume front is likely not captured correctly given the hydrostatic assumption utilized in these simulations. Convective instabilities there could create more mixing beyond what is determined in the current experiments and subsequently change the plume footprint and transport. All river plume instabilities are parameterized by the hydrostatic assumption, but the mixing induced by the smaller vertical displacements of Kelvin–Helmholtz and similar instabilities landward of the front are captured sufficiently (MacDonald et al., 2007) relative to the larger

SPICER ET AL. 17 of 21



### Journal of Geophysical Research: Oceans

10.1029/2022JC018462

convective instabilities at the front itself. Even at the front, hydrostatic models have been shown to reproduce dynamics reasonably well (O'Donnell et al., 1998).

Numerical mixing of tracers (such as salt) can be created due to discretization errors of tracer advection schemes in numerical ocean models (Burchard & Rennau, 2008). This phenomenon is physically unreal and can result in spurious additional mixing. In the calculations presented, the dissipation term from Equation 3 directly calculates physical mixing and so our estimates of mixing omit numerical errors. That said, numerical mixing can still indirectly modify vertical salinity gradients which consequently modify straining and mixing estimates (Burchard & Rennau, 2008), and so is important to mention. Here, we quantified numerical mixing as the residual of the balance given in Equation 3. Generally, the numerical mixing is small (<30%) relative to physical mixing (dissipation of vertical variance) during the study period (Figure 9b) but can become enhanced (>50%) during some strong straining/mixing events. This is in-line with the findings of Rennau (2011), who found numerically induced mixing may be of similar magnitude to physical mixing when modeling the advection of larger density gradients, such as those around a river plume or stratified estuary. Increasing the horizontal resolution of hydrostatic models has been shown to reduce numerical mixing by better representing sharp salinity gradients (Burchard et al., 2021).

#### 5. Conclusions

During winds which create surface flow opposing Kelvin wave propagation (typically northward), the Merrimack River plume and ambient shelf stratification advect offshore. Instantaneous wind generally dictates plume and ambient shelf stratification transport due to the short, tidal time scale of plume development, and relatively small spatial scales of spreading which prevent subtidal Ekman dynamics from taking influence over the shallow, frictional shelf. Collectively, a relatively homogenous, salty shelf condition is created nearshore. Saltier water beneath the plume creates larger density gradients at the plume base while offshore-directed surface currents increase straining, thereby increasing interfacial mixing intensity in the near- and midfield plume relative to other wind directions. Dissipation of vertical variance was found to peak in magnitude on the tide following a northward wind event when straining was less intense, but the shelf was set to a saltier ambient condition, outlining the greater influence of shelf stratification to mixing than straining.

During winds with a southward component or light wind scenarios, the Merrimack River plume behaves as a "typical" tidal plume, spreading out from the river mouth then rotating downcoast due to Coriolis. Advection accumulates excess stratification on the shelf nearshore and straining in the near- and midfield is unenhanced as wind-induced surface velocities oppose the plume and slow offshore propagation, decreasing shear in the plume interior relative to the northward wind case. Less wind straining and a deeper plume base create a less intense interfacial mixing environment between plume and ambient water.

This is the first study providing an evaluation of tidal time scale, realistic wind effects on nearfield and midfield mixing in a medium-sized tidally pulsed river plume. Analysis shows the importance of winds in dictating ambient shelf stratification and plume straining, both of which act as controls on mixing (dissipation of variance) in the interior plume. The results of this work are important to consider for future modeling of tracers from land to sea, as transport and mixing can be strongly connected to the wind, even in tidal plumes.

#### **Appendix A: Depth Effects on Salinity Variance**

Here, we expand on how stratification is quantified via vertical salinity variance and what to consider when interpreting it. Consider a plume underlain by a relatively shallow, salty shelf (Figure A1a) relative to the same plume over a deeper shelf of the same salinity (Figure A1b). The vertical average of salinity,  $\overline{S}$  (and the salinity which would comprise the entire water column if fully mixed) will be greater for the plume over deeper water (Figure A1, right panels), subsequently increasing the depth-averaged and integrated values of  $(S'_v)^2$ . Although the density gradient between plume and salty water is unchanged, it would take more mixing to homogenize the deeper water column and so  $\int (S'_v)^2 dz$  scales up (not unlike stratification quantified via the PEA [Simpson et al., 1990]). Similarly, most terms in Equation 3 (net rate of change, advection, and straining) would increase over the deeper water column to hold the conservation of  $(S'_v)^2$ . In this work, Equations 1–3 are quantified from

SPICER ET AL. 18 of 21

21699291, 2022, 5, Downloaded from https://agupubs.onlinelibrary.wiley.com/doi/10.1029/2022IC018462, Wiley Online Library on [09/05/2023]. See the Terms and Conditions (https://onlinelibrary.wiley.com/term/

articles are governed by the applicable Creative Commons License

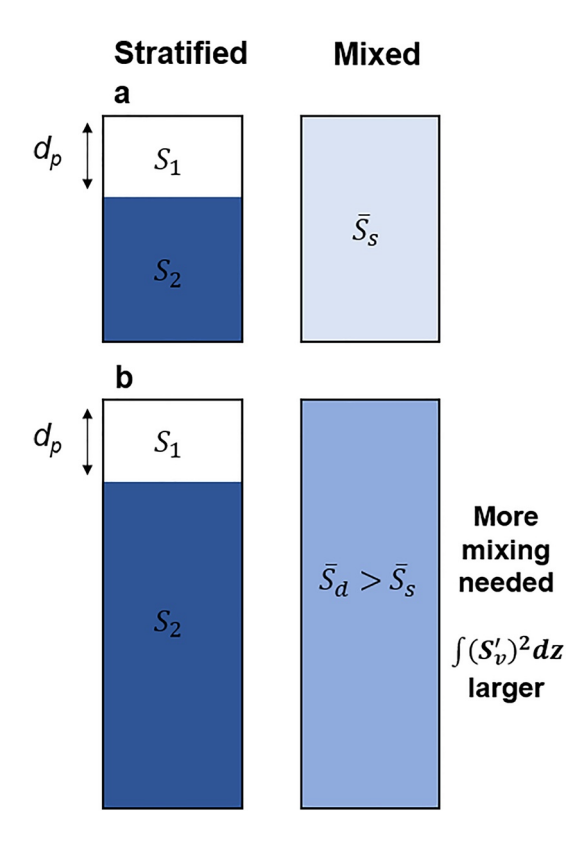


Figure A1. Conceptual schematic of plume of thickness  $d_p$  and salinity  $S_1$  overlaying relatively saltier water (salinity  $S_2$ ) for a (a) shallow and (b) deep shelf (left panels). Final water column salinity assuming full mixing is shown for each (right panels) and equals the depth average of left panel salinities:  $\overline{S}_s$  for shallow and  $\overline{S}_d$  for deep. Color scales with salinity (white is fresh, dark blue is saltiest). Differing final, mixed water column salinities indicates differing  $\int (S_p')^2 dz$  (stratification).

surface to bottom, and so variation in terms from sloping bathymetry exists and is valid given the definition of stratification we present here. By analyzing a control volume of nearly constant size (some tidal variability, discussed below), we are intercomparing the same depth range on the shelf and so variation is relative to that volume.

In the analysis presented in this paper, there is still some potential for depth-derived variance variation to affect results, which is worth addressing here. Variation to water level from tides can effectively modify the control volume and therefore bias bulk variance quantities at a tidal time scale, while comparing different plumes which spread over nonidentical spatial scales introduces a similar issue. We evaluated the importance of depth bias by quantifying  $\int \int (S'_v)^2 dx \, dy \, dz$  and  $\int (S'_v)^2 dz$  for two idealized scenarios using the same horizontal area as our control volume ( $\sim$ 225 km²), but modified depths for a high tide case (25 m total depth) and low tide case (22 m total depth). These depths were chosen as they are near the average depth of the control volume we utilize (Figure 1) and show sea level variability which is typical of the Merrimack outflow. A salinity profile representative of average conditions was applied over each domain and features a linear decrease from 15 psu at the surface to 30 psu at 4 m, with the remainder of the water column set to 32 psu. The difference in  $\int \int \int (S'_v)^2 dx \, dy \, dz$  due to depth variation was less than 2 psu² km³ ( $\sim$ 3% difference) while differences in  $\int (S'_v)^2 dz$  were less than 10 psu² m ( $\sim$ 2% difference), both of which are considered negligible relative to variation from straining, advection, and mixing, which can create differences which are orders of magnitude apart (see Section 3).

The salinity coordinate approach utilized in Section 3 tracks different plume salinity classes regardless of depth, possibly introducing some depth-derived bias to the results presented in Figure 6. In particular, we would expect salinity classes (plume regions) which advect over significantly different depth ranges between plume SW and NE to be most influenced. In Figure 3, the 20–25 psu salinity class corresponds to the periphery of the plume and exhibits the most spatial change between SW (large region nearshore, in depths <10 m) and NE (large region

SPICER ET AL. 19 of 21

21699291, 2022, 5, Downloaded from https://agupubs.onlinelibrary.wiley.com/doi/10.1029/2022IC018462, Wiley Online Library on [09/05/2023]. See

offshore, in depths >20 m). If significant, this variation in depth would skew straining and mixing intensities up in the 20–25 psu class during plume NE relative to SW in Figure 6. This does not occur, as intensities are similar or smaller, indicating minor bias in results.

#### **Data Availability Statement**

The original contributions presented in this study are publicly available. These data can be found at https://doi.org/10.5281/zenodo.6383185.

#### Acknowledgments

This project was funded by National Science Foundation Awards #1756690, #1756599, and #1756578. The authors would like to thank Steve Cousins and the rest of the Advanced Computing Group at the University of Maine for access to high-performance computing machines and support. We also thank Sam Kastner and another anonymous reviewer for thoughtful input on the original manuscript which greatly improved the end product.

#### References

- Burchard, H., Gräwe, U., Klingbeil, K., Koganti, N., Lange, X., & Lorenz, M. (2021). Effective diahaline diffusivities in estuaries. *Journal of Advances in Modeling Earth Systems*, 13, 2020MS002307. https://doi.org/10.1029/2020MS002307
- Burchard, H., & Hofmeister, R. (2008). A dynamic equation for the potential energy anomaly for analysing mixing and stratification in estuaries and coastal seas. *Estuarine, Coastal and Shelf Science*, 77, 679–687. https://doi.org/10.1016/j.ecss.2007.10.025
- Burchard, H., & Rennau, H. (2008). Comparative quantification of physically and numerically induced mixing in ocean models. *Ocean Modelling*, 20(3), 293–311. https://doi.org/10.1016/j.ocemod.2007.10.003
- Canuto, V. M., Howard, A., Cheng, Y., & Dubovikov, M. S. (2001). Ocean turbulence. Part I: One-point closure model—Momentum and heat vertical diffusivities. *Journal of Physical Oceanography*, 31(6), 1413–1426. https://doi.org/10.1175/1520-0485(2001)031<1413:OTPIOP>2.0.CO:2
- Chen, F., MacDonald, D. G., & Hetland, R. D. (2009). Lateral spreading of a near-field river plume: Observations and numerical simulations. Journal of Geophysical Research, 114, C07013. https://doi.org/10.1029/2008JC004893
- Chen, S. Y., & Chen, S. N. (2017). Generation of upwelling circulation under downwelling-favorable wind within bottom-attached, buoyant coastal currents. *Journal of Physical Oceanography*, 47, 2499–2519. https://doi.org/10.1175/JPO-D-16-0271.1
- Cole, K. L., MacDonald, D. G., Kakoulaki, G., & Hetland, R. D. (2020). River plume source-front connectivity. Ocean Modelling, 150, 101571. https://doi.org/10.1016/j.ocemod.2020.101571
- de Boer, G. J., Pietrzak, J. D., & Winterwerp, J. C. (2008). Using the potential energy anomaly equation to investigate tidal straining and advection of stratification in a region of freshwater influence. *Ocean Modelling*, 22, 1–11. https://doi.org/10.1016/j.ocemod.2007.12.003
- Flater, D. (2005). XTide: Harmonic tide clock and tide predictor. Retrieved from https://flaterco.com/xtide/
- Flather, R. A. (1975). A tidal model of the north-west European continental shelf. In Mémoires de la Société royale des sciences de Liège, Ser. 6.
  Flores, R. P., Rijnsburger, S., Horner-Devine, A. R., Souza, A. J., & Pietrzak, J. D. (2017). The impact of storms and stratification on sediment transport in the Rhine region of freshwater influence. Journal of Geophysical Research: Oceans, 122, 4456–4477. https://doi.org/10.1002/2016JC012362
- Fong, D. A., & Geyer, W. (2001). Response of a river plume during an upwelling favorable wind event. *Journal of Geophysical Research*, 106(C1), 1067–1084. https://doi.org/10.1029/2000JC900134
- Fong, D. A., Geyer, W. R., & Signell, R. P. (1997). The wind-forced response on a buoyant coastal current: Observations of the western Gulf of Maine plume. *Journal of Marine Systems*, 12(1–4), 69–81. https://doi.org/10.1016/S0924-7963(96)00089-9
- Garvine, R. W. (1987). Estuary plumes and fronts in shelf waters: A layer model. Journal of Physical Oceanography, 17(11), 1877–1896. https://doi.org/10.1175/1520-0485(1987)017<1877:EPAFIS>2.0.CO:2
- Gerbi, G. P., Chant, R. J., & Wilkin, J. L. (2013). Breaking surface wave effects on river plume dynamics during upwelling-favorable winds. Journal of Physical Oceanography, 43, 1959–1980. https://doi.org/10.1175/JPO-D-12-0185.1
- Gerbi, G. P., Kastner, S. E., & Brett, G. (2015). The role of whitecapping in thickening the ocean surface boundary layer. *Journal of Physical Oceanography*, 45(8), 2006–2024. https://doi.org/10.1175/JPO-D-14-0234.1
- Geyer, W. R., Scully, M. E., & Ralston, D. K. (2008). Quantifying vertical mixing in estuaries. Environmental Fluid Mechanics, 8, 495–509. https://doi.org/10.1007/s10652-008-9107-2
- Geyer, W. R., Signell, R. P., Fong, D. A., Wang, J., Anderson, D. M., & Keafer, B. A. (2004). The freshwater transport and dynamics of the Western Maine Coastal Current. Continental Shelf Research, 24(12), 1339–1357. https://doi.org/10.1016/j.csr.2004.04.001
- Haidvogel, D. B., Arango, H., Budgell, W. P., Cornuelle, B. D., Curchitser, E., Di Lorenzo, E., et al. (2008). Ocean forecasting in terrain-following coordinates: Formulation and skill assessment of the Regional Ocean Modeling System. *Journal of Computational Physics*, 227(7), 3595–3624. https://doi.org/10.1016/j.jcp.2007.06.016
- Hetland, R. D. (2005). Relating river plume structure to vertical mixing. Journal of Physical Oceanography, 35(9), 1667–1688. https://doi.org/10.1175/JPO2774.1
- Hetland, R. D. (2010). The effects of mixing and spreading on density in near-field river plumes. *Dynamics of Atmospheres and Oceans*, 49(1), 37–53. https://doi.org/10.1016/j.dynatmoce.2008.11.003
- Hetland, R. D., & MacDonald, D. G. (2008). Spreading in the near-field Merrimack River plume. Ocean Modelling, 21(1), 12–21. https://doi.org/10.1016/j.ocemod.2007.11.001
- Hickey, B. M., Kudela, R. M., Nash, J. D., Bruland, K. W., Peterson, W. T., MacCready, P., et al. (2010). River influences on shelf ecosystems: Introduction and synthesis. *Journal of Geophysical Research*, 115, C00B17. https://doi.org/10.1029/2009JC005452
- Hickey, B. M., Pietrafesa, L. J., Jay, D. A., & Boicourt, W. C. (1998). The Columbia River Plume Study: Subtidal variability in the velocity and salinity fields. *Journal of Geophysical Research*, 103(C5), 10339–10368. https://doi.org/10.1029/97JC03290
- Horner-Devine, A. R., Hetland, R. D., & MacDonald, D. G. (2015). Mixing and transport in coastal river plumes. Annual Review of Fluid Mechanics, 47, 569–594. https://doi.org/10.1146/annurev-fluid-010313-141408
- Horner-Devine, A. R., Jay, D. A., Orton, P. M., & Spahn, E. Y. (2009). A conceptual model of the strongly tidal Columbia River plume. *Journal of Marine Systems*, 78(3), 460–475. https://doi.org/10.1016/j.jmarsys.2008.11.025
- Huguenard, K. D., Bogucki, D. J., Ortiz-Suslow, D. G., Laxague, N. J. M., MacMahan, J. H., Özgökmen, T. M., et al. (2016). On the nature of the frontal zone of the Choctawhatchee Bay plume in the Gulf of Mexico. *Journal of Geophysical Research: Oceans*, 121, 1322–1345. https://doi.org/10.1002/2015JC010988

SPICER ET AL. 20 of 21



#### Journal of Geophysical Research: Oceans

- 10.1029/2022JC018462
- Hunter, E. J., Chant, R. J., Wilkin, J. L., & Kohut, J. (2010). High-frequency forcing and subtidal response of the Hudson River plume. *Journal of Geophysical Research*, 115, C07012. https://doi.org/10.1029/2009JC005620
- Jurisa, J. T., & Chant, R. J. (2013). Impact of offshore winds on a buoyant river plume system. Journal of Physical Oceanography, 43(12), 2571–2587. https://doi.org/10.1175/JPO-D-12-0118.1
- Kakoulaki, G. (2015). Using Lagrangean surface drifters to study wind forcing and lateral spreading in a buoyant river plume (thesis). North Dartmouth. MA: University of Massachusetts Dartmouth.
- Kakoulaki, G., Macdonald, D., & Horner-Devine, A. R. (2014). The role of wind in the near field and midfield of a river plume. *Geophysical Research Letters*, 41, 5132–5138. https://doi.org/10.1002/2014GL060606
- Kalra, T. S., Li, X., Warner, J. C., Geyer, W. R., & Wu, H. (2019). Comparison of physical to numerical mixing with different tracer advection schemes in estuarine environments. *Journal of Marine Science and Engineering*, 10(7), 338. https://doi.org/10.3390/jmse7100338
- Kämpf, J. (2015). Interference of wind-driven and pressure gradient-driven flows in shallow homogeneous water bodies. *Ocean Dynamics*, 65(11), 1399–1410. https://doi.org/10.1007/s10236-015-0882-2
- Kämpf, J. (2017). Wind-driven overturning, mixing and upwelling in shallow water: A nonhydrostatic modeling study. *Journal of Marine Science and Engineering*, 5(4), 47. https://doi.org/10.3390/jmse5040047
- Kastner, S. E., Horner-Devine, A. R., & Thomson, J. (2018). The influence of wind and waves on spreading and mixing in the Fraser River plume. Journal of Geophysical Research: Oceans, 123, 6818–6840. https://doi.org/10.1029/2018JC013765
- Lentz, S. (2004). The response of buoyant coastal plumes to upwelling-favorable winds. *Journal of Physical Oceanography*, 34(11), 2458–2469. https://doi.org/10.1175/JPO2647.1
- Lentz, S., & Fewings, M. R. (2012). The wind- and wave-driven inner-shelf circulation. Annual Review of Marine Science, 4, 317–343. https://doi.org/10.1146/annurev-marine-120709-142745
- Li, X., Geyer, W. R., Zhu, J., & Wu, H. (2018). The transformation of salinity variance: A new approach to quantifying the influence of straining and mixing on estuarine stratification. *Journal of Physical Oceanography*, 48(3), 607–623. https://doi.org/10.1175/JPO-D-17-0189.1
- MacCready, P., Geyer, W. R., & Burchard, H. (2018). Estuarine exchange flow is related to mixing through the salinity variance budget. *Journal of Physical Oceanography*, 48(6), 1375–1384. https://doi.org/10.1175/JPO-D-17-0266.1
- MacDonald, D. G., Goodman, L., & Hetland, R. D. (2007). Turbulent dissipation in a near-field river plume: A comparison of control volume and microstructure observations with a numerical model. *Journal of Geophysical Research*, 112, C07026. https://doi.org/10.1029/2006JC004075
- Moffat, C., & Lentz, S. (2012). On the response of a buoyant plume to downwelling-favorable wind stress. *Journal of Physical Oceanography*, 42(7), 1083–1098. https://doi.org/10.1175/JPO-D-11-015.1
- Monismith, S. G. (2010). Mixing in estuaries. In A. Valle-Levinson (Ed.), Contemporary issues in estuarine physics (pp. 145–185). New York: Cambridge University Press.
- Nash, J. D., Kilcher, L. F., & Moum, J. N. (2009). Structure and composition of a strongly stratified, tidally pulsed river plume. *Journal of Geophysical Research*, 114, C00B12. https://doi.org/10.1029/2008JC005036
- O'Donnell, J., Marmorino, G. O., & Trump, C. L. (1998). Convergence and downwelling at a river plume front. *Journal of Physical Oceanogra-phy*, 28(7), 1481–1495. https://doi.org/10.1175/1520-0485(1998)028<1481:CADAAR>2.0.CO;2
- Orlanski, I. (1976). A simple boundary condition for unbounded hyperbolic flows. Journal of Computational Physics, 21(3), 251–269. https://doi.org/10.1016/0021-9991/76)90023-1
- Pritchard, M., & Huntley, D. A. (2006). A simplified energy and mixing budget for a small river plume discharge. *Journal of Geophysical Research*, 111, C03019. https://doi.org/10.1029/2005JC002984
- Ralston, D. K., Geyer, W. R., Lerczak, J. A., & Scully, M. (2010). Turbulent mixing in a strongly forced salt wedge estuary. *Journal of Geophysical Research*, 115, C12024. https://doi.org/10.1029/2009IC006061
- Rennau, H. (2011). Natural, numerical and structure-induced mixing in dense gravity currents: Idealised and realistic model studies. Rostock, Germany: University of Rostock.
- Rijnsburger, S., Flores, R. P., Pietrzak, J. D., Horner-Devine, A. R., & Souza, A. J. (2018). The influence of tide and wind on the propagation of fronts in a shallow river plume. *Journal of Geophysical Research: Oceans.* 123, 5426–5442. https://doi.org/10.1029/2017JC013422
- Scully, M. E., Friedrichs, C., & Brubaker, J. (2005). Control of estuarine stratification and mixing by wind-induced straining of the estuarine density field. Estuaries, 28(3), 321–326. https://doi.org/10.1007/BF02693915
- Shchepetkin, A. F., & McWilliams, J. C. (2005). The regional oceanic modeling system (ROMS): A split-explicit, free-surface, topography-following-coordinate oceanic model. *Ocean Modelling*, 9(4), 347–404. https://doi.org/10.1016/j.ocemod.2004.08.002
- Simpson, J. H., Brown, J., Matthews, J., & Allen, G. (1990). Tidal straining, density currents, and stirring in the control of estuarine stratification. Estuaries, 13, 125–132. https://doi.org/10.2307/1351581
- Smolarkiewicz, P. K., & Grabowski, W. W. (1990). The multidimensional positive definite advection transport algorithm: Nonoscillatory option. Journal of Computational Physics, 86(2), 355–375. https://doi.org/10.1016/0021-9991(90)90105-A
- Spahn, E. Y., Horner-Devine, A. R., Nash, J. D., Jay, D. A., & Kilcher, L. (2009). Particle resuspension in the Columbia River plume near field. Journal of Geophysical Research, 114, C00B14. https://doi.org/10.1029/2008JC004986
- Spicer, P., Cole, K. L., Huguenard, K., MacDonald, D. G., & Whitney, M. M. (2021). The effect of bottom-generated tidal mixing on tidally pulsed river plumes. *Journal of Physical Oceanography*, 51(7), 2223–2241. https://doi.org/10.1175/JPO-D-20-0228.1
- Tilburg, C. E. (2003). Across-shelf transport on a continental shelf: Do across-shelf winds matter? *Journal of Physical Oceanography*, 33(12), 2675–2688. https://doi.org/10.1175/1520-0485(2003)033<2675:ATOACS>2.0.CO:2
- Umlauf, L., & Burchard, H. (2003). A generic length-scale equation for geophysical turbulence models. *Journal of Marine Research*, 61(2), 235–265. https://doi.org/10.1357/002224003322005087
- Warner, J. C., Geyer, W. R., Ralston, D. K., & Kalra, T. (2020). Using tracer variance decay to quantify variability of salinity mixing in the Hudson River estuary. *Journal of Geophysical Research: Oceans*, 125, e2020JC016096. https://doi.org/10.1029/2020JC016096
- Whitney, M. M., & Garvine, R. W. (2005). Wind influence on a coastal buoyant outflow. *Journal of Geophysical Research*, 110, C03014. https://doi.org/10.1029/20031C002261
- Zhang, Z., Hetland, R., & Zhang, X. (2014). Wind-modulated buoyancy circulation over the Texas–Louisiana shelf. *Journal of Geophysical Research: Oceans*, 119, 5705–5723. https://doi.org/10.1002/2013JC009763

SPICER ET AL. 21 of 21